Electronic ISSN: 1309-0267

I J E A S

International Journal of Engineering & Applied Sciences

IJEAS

Volume 13, Issue 1
2021

Published by Akdeniz University

Editorial Board

(The name listed below is not Alphabetical or any title scale)

Abstracting & Indexing

IJEAS provides unique DOI link to every paper published.

Editorial Scope

The journal presents its readers with broad coverage across some branches of engineering and science of the latest development and application of new solution algorithms, artificial intelligent techniques innovative numerical methods and/or solution techniques directed at the utilization of computational methods in solid and nano-scaled mechanics.

International Journal of Engineering & Applied Sciences (IJEAS) is an Open Access Journal

International Journal of Engineering & Applied Sciences (IJEAS) publish original contributions on the following topics:

Numerical Methods in Solid Mechanics

Nanomechanic and applications

Microelectromechanical systems (MEMS)

Vibration Problems in Engineering

Higher order elasticity (Strain gradient, couple stress, surface elasticity, nonlocal elasticity) Applied Mathematics

IJEAS allows readers to read, download, copy, distribute, print, search, or link to the full texts of articles.

CONTENTS

International Journal of Engineering & Applied Sciences (IJEAS)
Vol. 13, Issue 1 (2021) 1-9
http://dx.doi.org/10.24107/ijeas.840991
Int J Eng Appl Sci 13(1) (2021) 1-9

Analysis of the Effects of Capacitances on Transformers in Transient Regimes by Finite Element Method

Yıldırım Özüpak

Dicle University Silvan Vocational School, Electrical and Energy Department, Diyarbakır, Turkey
E-mail address: yildirim.ozupak@dicle.edu.tr

ORCID numbers of author:
0000-0001-8461-8702

Received date: 15.12.2020
Accepted date: 29.01.2021

Abstract

High currents occurring in transformers in transient state may cause the insulation materials to deteriorate. In this paper, the effects of the capacitance values between the winding and the core and between the windings on the transition of the lightning strike applied to the secondary side to the primary side of power transformers were analyzed. Transformer models were created in ANSYS@Maxwell-2D environment, which realizes a solution based on Finite Element Method (FEM). In simulation studies, a lightning impulse voltage of 1/100 µs was applied to the secondary side of the transformer with a special method. It has been observed that the change of the values of the capacitances between the windings in power transformers affects the amplitude of the primary lightning impulse voltage. With this study, the weak points of the insulation materials of transformers windings were determined and the electric field distribution was analyzed.

Keywords: Transformer, FEM, Lightning Impulse, Electric field, Maxwell-2D.

1. Introduction

Transformer models can be classified as low frequency [1] and high frequency [2] models according to the applied source frequency. Low frequency models are created by open and short circuit tests. Studies on low frequency model aim to model the nonlinear characteristics of the core [3]. High frequency model studies are carried out for fault detection of transformers and analysis of transient response [4]. In these models, which are analyzed based on high frequency, capacitances are added to the designs in addition to the parameters in the low frequency model. Since the effect of these capacitances at low frequencies is negligible, they are not included in the analysis. However, at high frequencies these capacitances significantly affect the transformer output.

Experimental tests have been performed on the current transformer in [3], among the studies on the lightning impulse response of transformers, and the lightning impulse response has been measured. With the test results, the equivalent circuit and transfer function of the transformer are established. The lightning impulse response measured with the simulation results with the model designed in ANSYS @ Maxwell environment was compared. In [4] the Frequency Response Analysis (FRA) method and an advanced model of the frequency response of a three-phase power transformer are presented to be used for fault detection. In

[5], the power transformer and distribution transformer have been tested with FRA (Frequency Response Analysis) device and the equivalent circuits of the transformers have been removed. In [6], a simple modeling method based on measurement data in frequency domain, which can be easily applied in Electromagnetic Transients Program (EMTP) for power transformer, is tried to be presented. The important function of the model is that it can simulate the transient voltage transferred from one winding to another after lightning strike or switching.

In this paper, in the power transformer model in [5], the effect of the change of capacitance values on the primary side in case of a lightning strike applied to the secondary side has been investigated. Transformer models were created in ANSYS@Maxwell program. The electric field analysis of the model and the voltage distribution on the transformer are examined.

2. Power Transformer Model

[5] Study derives the power transformer model from study [6]. Experimental tests were carried out by applying 1.2/50 μs lightning strikes to a 300 MVA 415/15.75kV Y-Δ power transformer. Fig. 1 shows the power transformer model.

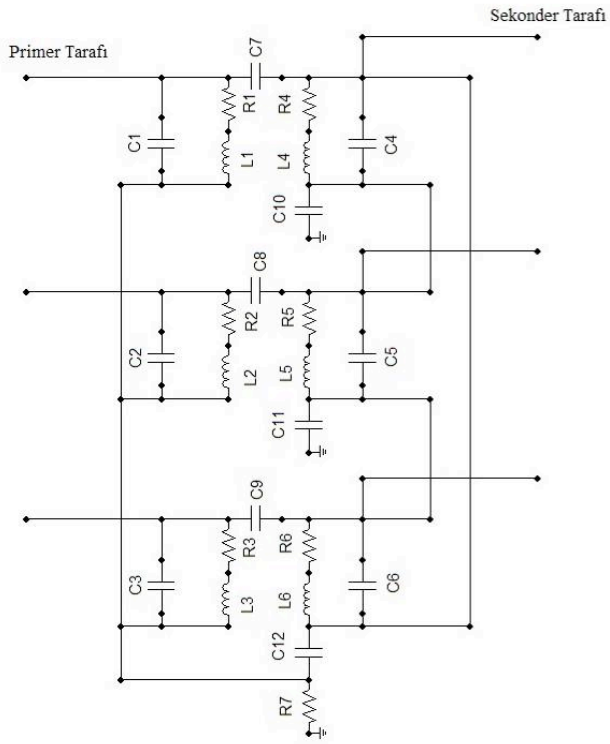

Fig. 1. High frequency power transformer model [5]

Copper losses are not taken into account in this model. C_1-C_6 coil capacitances; C_7, C_8 and C9 capacitances between windings; C_{10}, C_{11} and C_{12} represent the capacitance between the neutral point and ground. R_1-R_6 and L_1-L_6 represent iron losses (magnetic circuit). R7 represents the neutral resistance.

Fig. 2 contains the test setup required for the measurement of the frequency response analysis (FRA) winding impedance of Primary - Earth (V_{in}) and Neutral - Earth (V_{out}) voltages [6]. By using the frequency spectrum of the winding impedance amplitude and angle, magnetic circuit resistance and inductance and winding capacitance can be obtained [6]. Since impedance is inductive at low frequencies, the winding capacitance can be regarded as open circuit and thus the magnetic circuit inductance can be determined from the measured reactance value. The winding capacitance is calculated using the inductance found in the first resonance frequency and low frequency calculation. In Eq. (1), the relation between voltages and winding impedance is given. In Eq. (2), the resonance frequency Eq. is given.

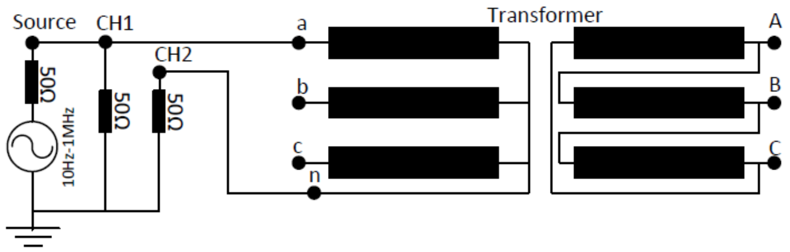

Fig. 2. Power transformer primary test setup [2]

$$Z_s = \frac{V_{out}}{V_{in}}.50 - 50 = 50.\left(\frac{1-He^{\theta}}{He^{\theta}}\right), \quad \frac{V_{out}}{V_{in}} = |H|\angle\theta = He^{\theta} \tag{1}$$

$$f_r = \frac{1}{2\pi\sqrt{(LC}} \tag{2}$$

The 50 Ω resistance in Eq. (1) is the internal resistance of the measuring device. The necessary parameters can be determined by creating the same test setup for the secondary winding. Secondary A phase test setup is given in Fig. 3 [2].

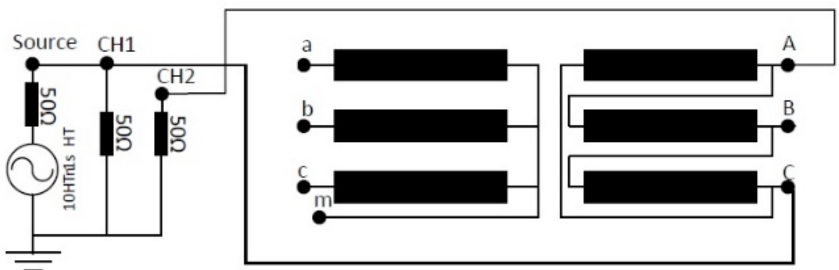

Fig. 3. Power transformer secondary test setup [2]

Primary and Secondary voltages were measured to determine the capacities between windings. In this study, it is stated that the frequency analysis of the primary and secondary voltages gives the impedance between the windings. At low frequencies, this impedance behaves capacitively and the capacitance value was obtained from the resistance [2]. Details of this test were not included in the study. The setup of this test is given in Fig. 4.

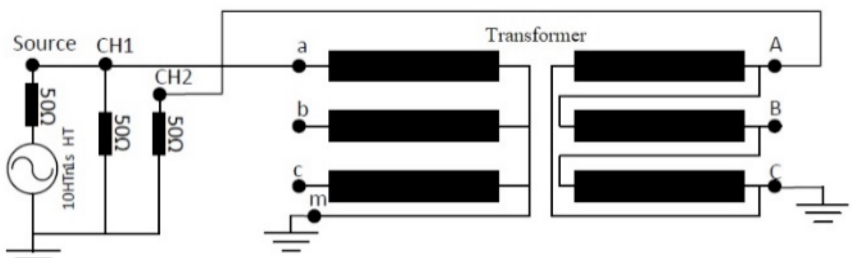

Fig. 4. Power transformer secondary-primary test setup [2]

In the model in [1], the capacitive effect of the primary side is transferred to the secondary side as leakage inductance due to the inductive coupling between the windings. In the frequency analysis of the secondary winding, it is seen that the impedance is inductive at the second resonance frequency. From the impedance value at this frequency, the inductance; From Eq. (2) capacitances can be found.

The parameters of the tests and calculations of the power transformer model given in Fig. 1 are given in Table 1. In this study, calculation of magnetic circuit resistances is not included. It can be understood from the study that these resistors are not removed from the low frequency impedance.

Table 1. Power Transformer Parameters [5]

R (Ω)	0.001053
L (H)	0.366
C12 (nF)	70.08

3. Modeling of Transformer Using ANSYS@Maxwell

Power transformer model in [5] were created in ANSYS@Maxwell environment and lightning impulse response was investigated. 170 kV 1/100 μs lightning impulse voltage was applied to the power transformer. The simulation is set to 100 μs. Lightning impulse has been applied in the 1st μs to see the voltage wave precisely. Fig. 5 shows the power transformer model.

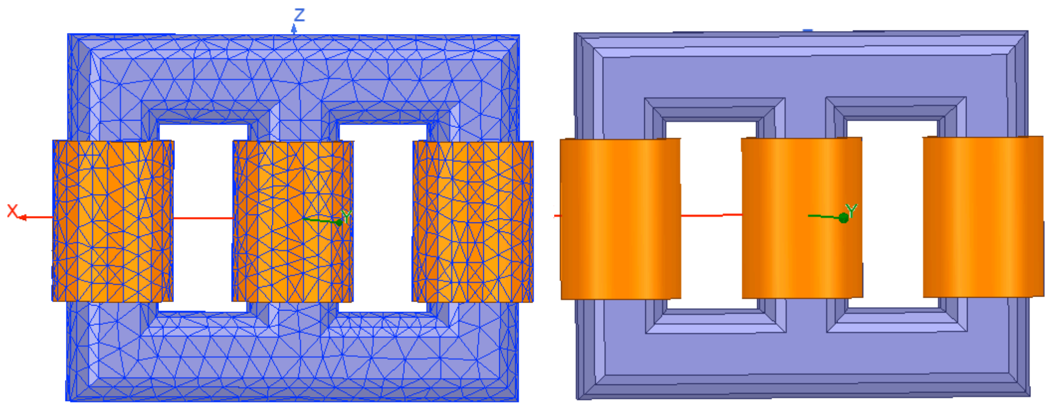

Fig. 5. Power transformer model

In the program environment, boundary conditions of the transformer model, geometric dimensions and the properties of all materials used are defined on the model. The core of the transformer is defined in the program environment with the B-H curve of the magnetic material and thin sheets. The B-H curve, which is the magnetic property of the core material used, is given in Fig. 6. The geometric properties of the designed transformer are given in Table 2.

Table 2. Geometric properties of the designed transformer

HV	33.000 V
LV	11.000 V
Core loss	12.500 W
Load loss	97.000 W
HV connection	Delta
LV connection	Star
HV turn number	675
LV turn number	131
HV current	152 A
LV currunt	785 A

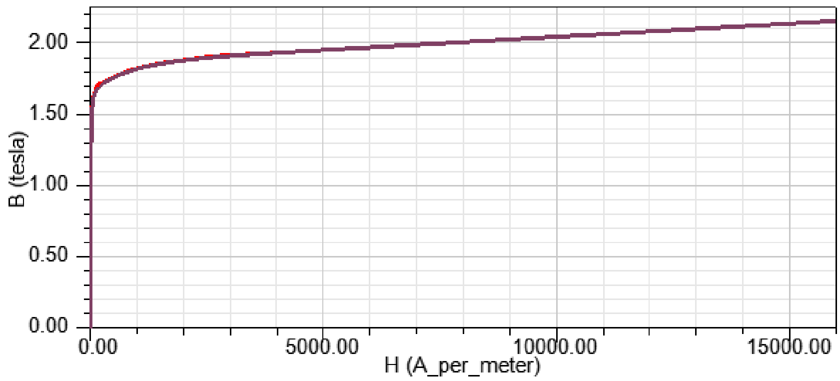

Fig. 6. B-H curve of core material

The graph of the lightning impulse voltage applied to the transformer windings in the program environment is presented in Fig. 7.

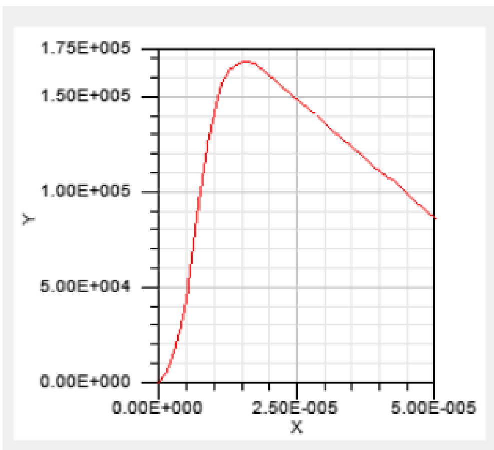

Fig. 7. Lightning impulse voltage applied.

3.1. Analysis of the model

In Fig. 7, the form of the voltage applied to the primary A phase of the power transformer, and the form of the voltage generated in the secondary. The electric field distribution caused by a lightning strike is given in Fig. 8. The electric field voltage curve is given in Fig. 9.

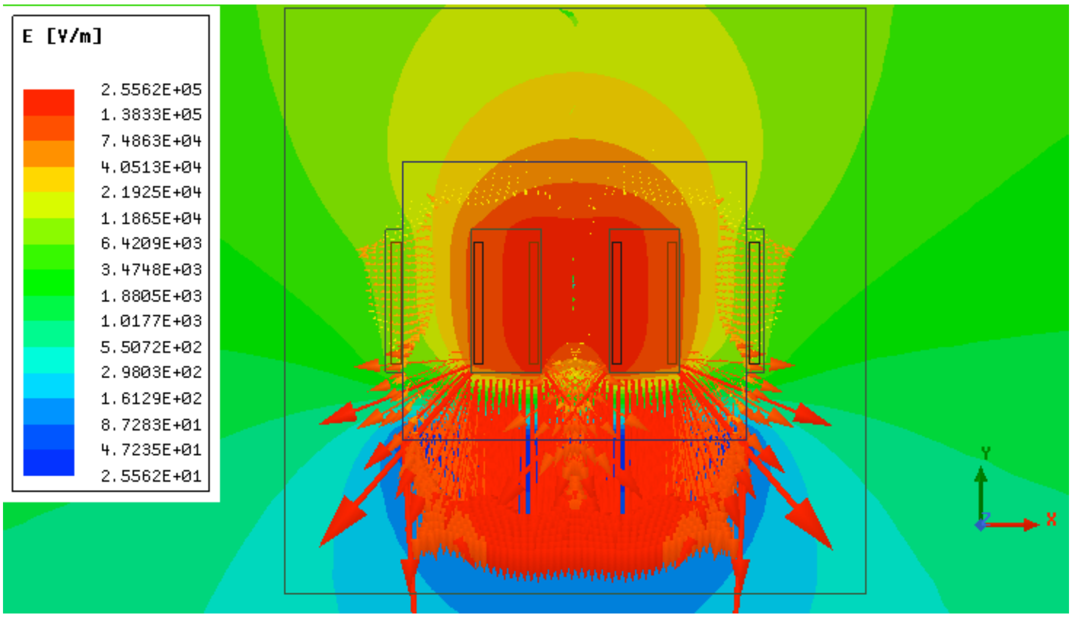

Fig. 8. Lightning-impulse electric field.

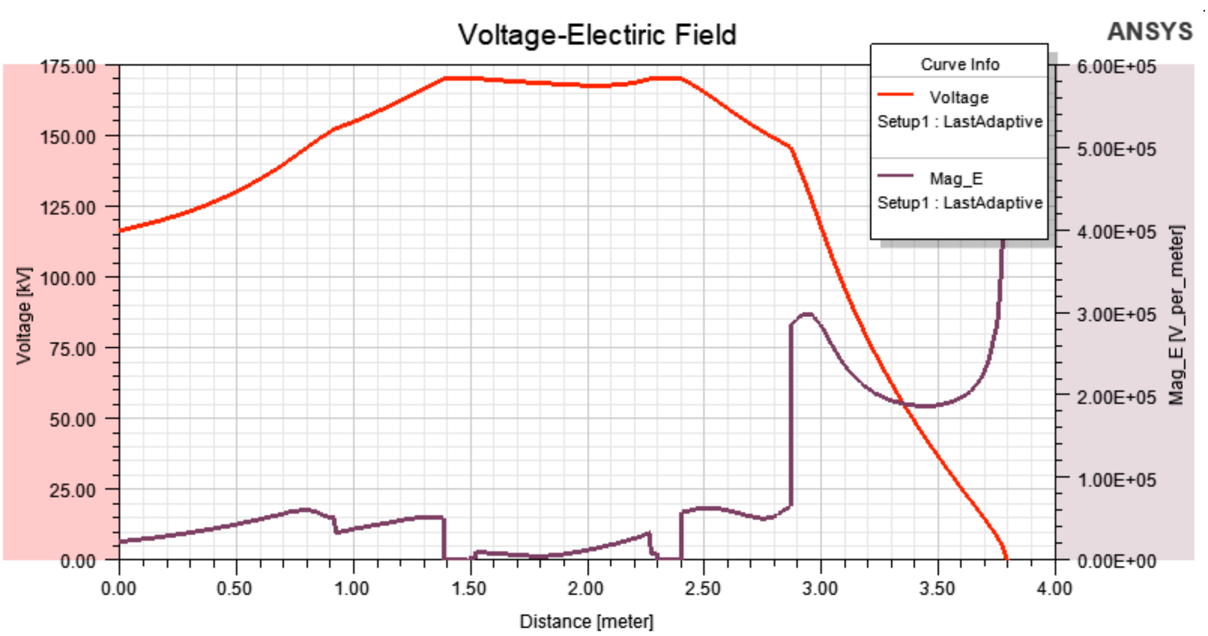

Fig. 9. Electric field-voltage relationship

The amplitude of the electric field value occurring in the transformer and the amplitude of the electric field strength are presented in Fig. 11 and Fig. 12, respectively.

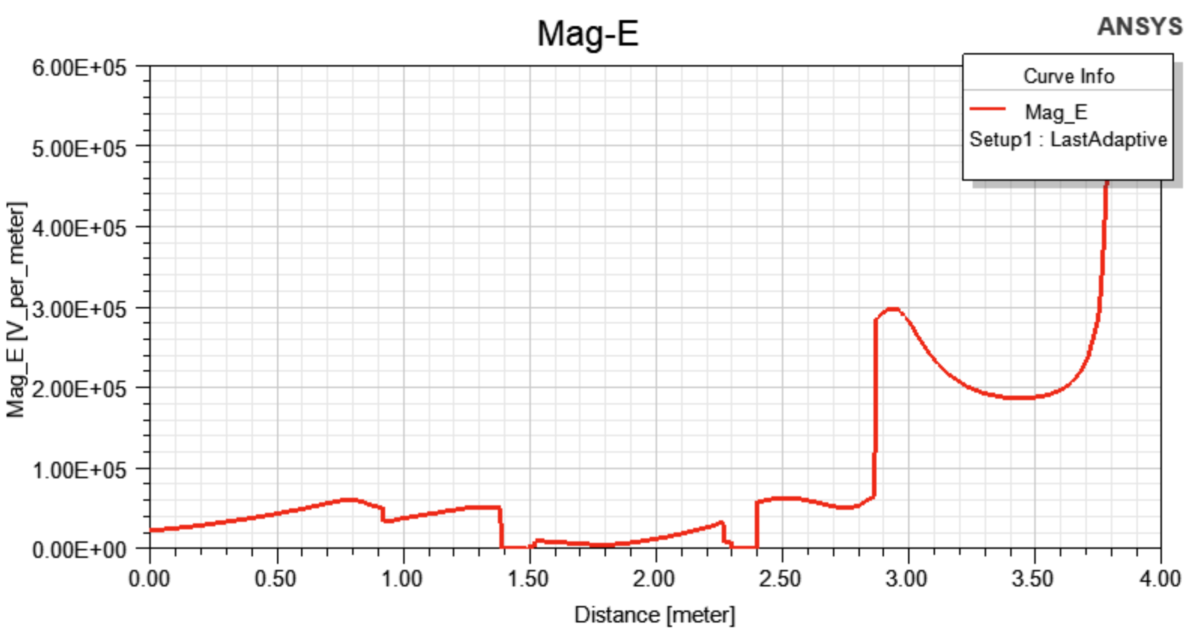

Fig. 10. Magnitude of electric field on primary winding.

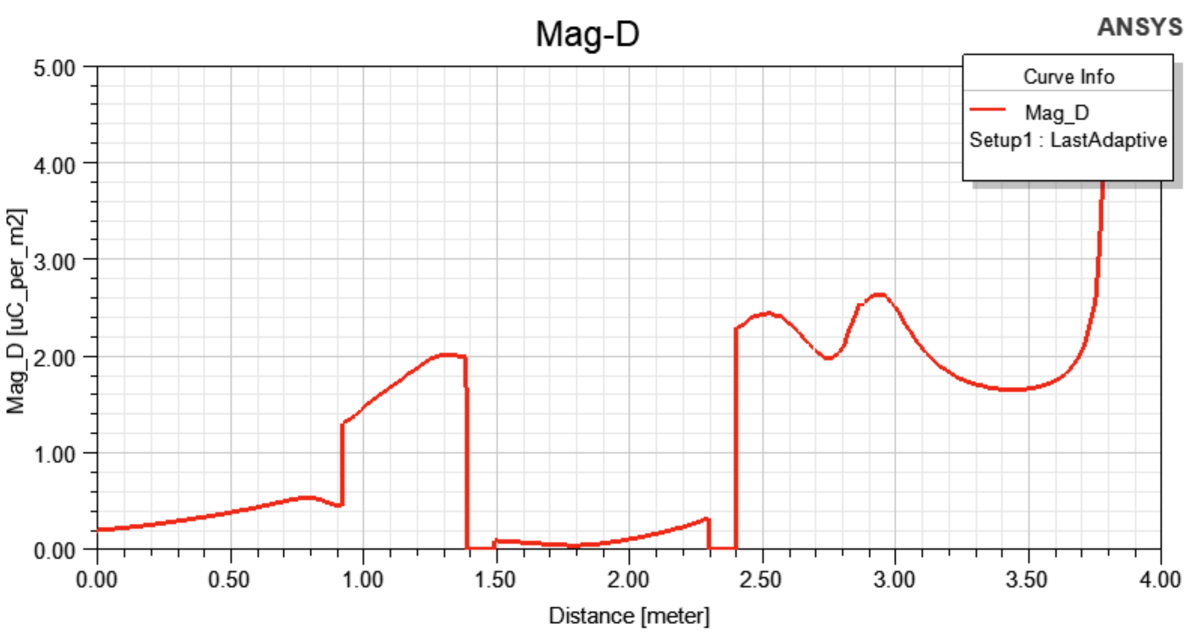

Fig. 11. Magnitude of density field

The energy released due to the electric field in the transformer windings and the stresses occurring at the edges of the transformer windings are given in Fig.s 12 and 13.

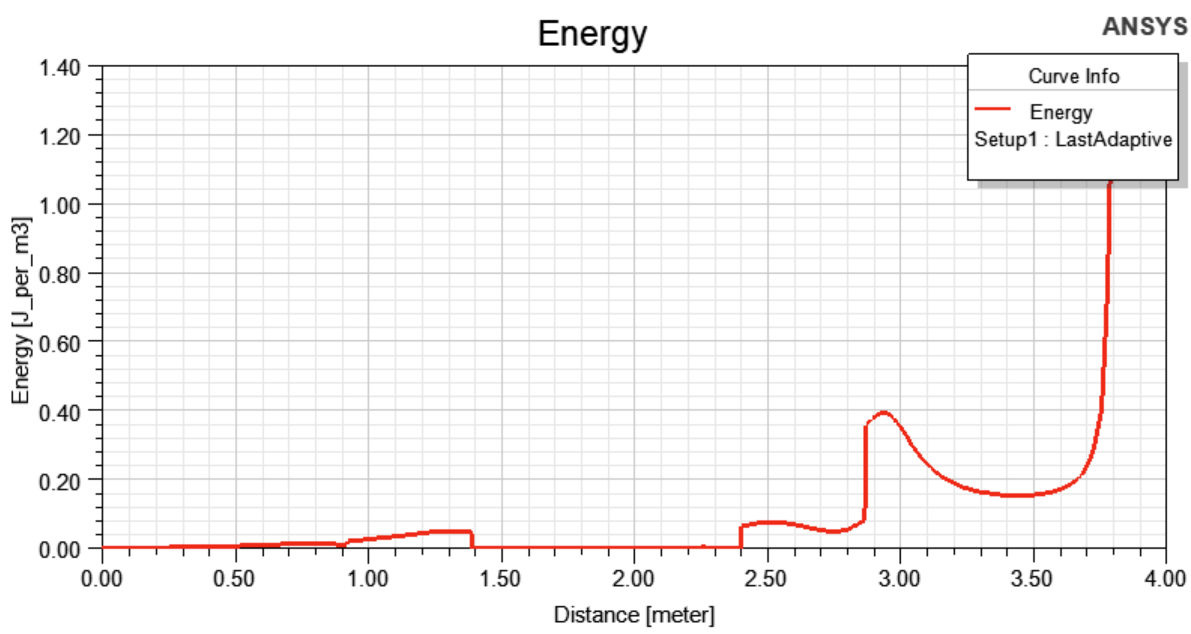

Fig. 12. Energy storage on winding

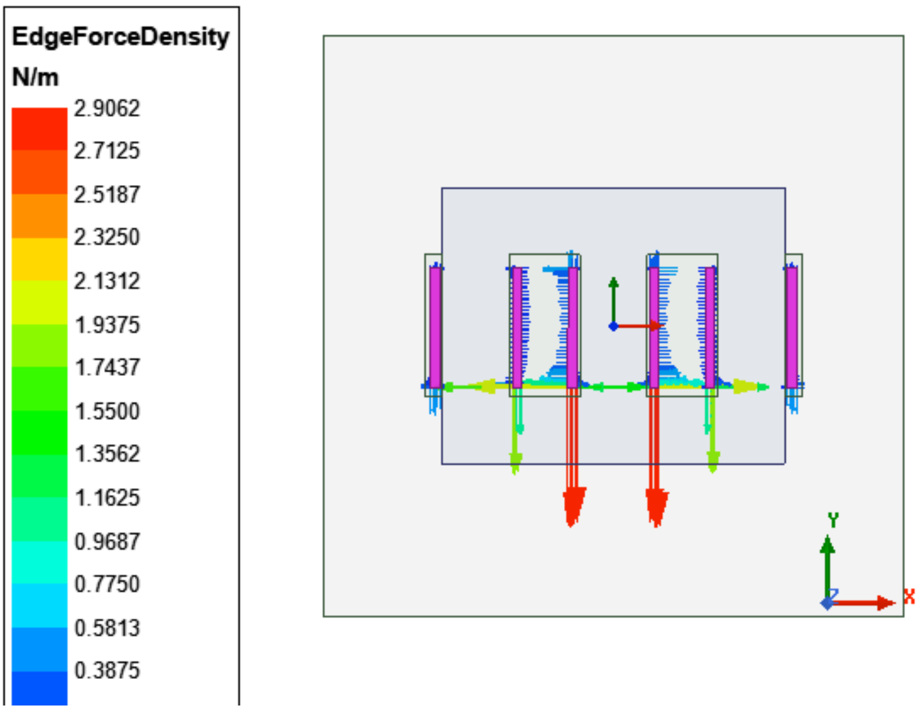

Fig. 13. Edge force density on winding

The result of the lightning voltage in the secondary winding is consistent with the lightning pulse applied. Critical areas that could cause degradation in the insulating materials between the primary and secondary windings have been identified. The electric field distribution in critical regions on the insulating material of the two-dimensional model is also shown.

7. Conclusions

In the power transformer model, it has been observed that changing capacitance values increase and decrease the amplitude of the voltage. In the conflict, it is also seen how the electric field of the transformer under transient regime causes the strain on the insulation material. Lightning impulse is a very important phenomenon for all electrical power systems due to surge surge. This is why the lightning analysis is equally important to the power problem. In this article, the lightning impulse voltage applied to the transformer during the lightning-strike, the electric field of the transformer and the voltage distribution are presented with simulation results. Critical areas between primary and secondary windings that may cause degradation in insulating materials are shown in three dimensions. The electric field distribution in critical regions on the insulation material of the two-dimensional model is also shown. This article presents the use of the integral Eq. approach in computing the electric field. This approach is used to solve a numerical example to verify the applicability of a transformer to calculate the electric field. The system of Eq.s is solved using boundary element methods. Results are compared to those of a commercial FEM software and are in good agreement.

Acknowledgments

This study was supported by Inonu University Scientific Research Projects Coordination Unit. Project Number: FBA-2017-639.

References

[1] Akdağ, M., Mamiş, M.S, Investigation the Effect of Capacitances on Lightning Impulse in Transformers, Güç Sistemleri Konferansi, 15-16 November, Ankara, 2018.

[2] Morched, A., Marti, L., Ottevangers, J., a high frequency transformer model for the EMTP, IEEE transactions on power delivery, 8(3), 1615-1626, 1993.

[3] Özüpak, Y., Mamiş, M.S, Teke, İ.H., Electromagnetic field and total loss analysis of transformers by finite element method, International Journal of Engineering And Computer Science, 8(1), 24451-24460, 2019.

[4] Özüpak, Y., Mamiş, M.S, Realization of electromagnetic flux and thermal analyses of transformers by finite element method, IEEJ Transactions on Electrical and Electronic Engineering, 14(10), 1478-1484, 2019.

[5] Subedi, D., Lightning induced over-voltages in power transformer and voltage spikes in connected load, Master Thesis, Aalto University, Helsinki, Finland, 2017.

[6] Shirvani, A., Malekian, K., Schmidt, U., Schufft, W., A new power transformer model over wide frequency range for EMTP, 45th International Universities Power Engineering Conference (UPEC2010), 1-6, 2010.

[7] Sabiha, N.A., Lightning-induced overvoltages in mediumvoltage distribution systems and customer experienced voltage spikes, PhD Thesis, Aalto University, Helsinki, Finland, 2010.

[8] Shareghi, M., Phung, B.T., Naderi, M.S., Blackburn, T.R., Ambikairajah, E., Effects of current and voltage harmonics on distribution transformer losses, International Conference on Condition Monitoring and Diagnosis (CMD), 633-636, 2012

[9] Soh, T.L.G., Said, D.M., Ahmad, N., Nor, K.M., Salim, F., Experimental study on the impact of harmonics on transformer, IEEE 7th International Power Engineering and Optimization Conference (PEOCO 2013), 686-690, 2013

International Journal of Engineering & Applied Sciences (IJEAS)
Vol. 13, Issue 1 (2021) 10-16
http://dx.doi.org/10.24107/ijeas.854437
Int J Eng Appl Sci 13(1) (2021) 10-16

An XAFS Study on the Electronic Structure Study of the Boron Substituted $CuFeO_2$

Osman Murat Ozkendir

Department of Natural and Mathematical Sciences, Faculty of Engineering, Tarsus University, Tarsus, Turkey
E-mail address: ozkendir@tarsus.edu.tr

ORCID numbers of authors:
0000-0002-0810-9938

Received date: 05.01.2021
Accepted date: 08.03.2021

Abstract

$CuFeO_2$ is a well known antiferromagnetic material with its geometrically frustrated antiferromagnetic (AFM) [T_N=11K] crystal. Besides, delafossite $CuFeO_2$ oxide crystal is known to be nonstoichiometric under the influence of oxygen as a result of the change in cation valence bands. In this study, boron atoms were substituted in the Fe coordination and the electronic response on irons valence band is probed. Due to the high difference in the ionic radii of the host and substituted atoms, different crystal structure formation was expected. However, calculations showed that boron atoms tend to locate in Fe coordination and preferred to be part of the host crystal by bonding with the oxygen atoms. In addition, the presence of the light boron atoms was determined to weaken the scattering intensities which cause a longer mean free path for the photoelectrons which means better conductivity of the material.

Keywords: Absorption; XAFS; Electronic Structure; Crystal Structure

1. Introduction

Transition metals have vast application in current technology due to their interesting electronic interactions with other metals that make them an active role player in molecular interplays. Their desired electronic and magnetic properties make them popular for many scientific studies such as their superior conductivity properties, magnetic sequences as well as their semiconductor properties (magnetic semiconductors). Also, the 3d elements are abundant in the earth's crust, and that means the commercially available powders are inexpensive and easy to use [1-5]. That's one of the reasons why the most popular magnetic materials of interest in the technological field are the ferromagnetic 3d transition metals, i.e., Fe, Co, and Ni, and their oxides. Low dimensional transition metal oxide $CuFeO_2$ is one of the popular members of the delafossite ABO_2 compounds, which is also one of the leading antiferromagnetic iron oxides with rhombohedral geometry and " R-3m" space group [T_N±11K) [6-9]. Delafossite $CuFeO_2$ is a remarkable magnetic material with its broken magnetic structure. The atomic structure of the delafossite group consists of a sheet of linearly coordinated “A” cations stacked between edge-shared octahedral layers (BO_6).

Studies on materials require a good scientific background and the right selection of the most appropriate techniques for the study. There are different techniques chosen to probe the different properties of the materials. But, one of the technique became popular with its useful data that can be used for several purposes, mainly for electronic structure and crystal structure, is the X-ray Absorption Fine Structure (XAFS) Spectroscopy. XAFS is a synchrotron radiation based technique and it can yield rich data that support the analysis of both crystal and electronic structure properties. The technique is one of the best tool to collect data on both single crystalline, polycrystalline, and non-crystalline materials. The XAFS data can be analyzed in two parts. The first part is called as the XANES (X-ray Absorption Near-Edge Spectroscopy) and the EXAFS (Extended-XAFS). Data of the XANES region on the XAFS spectra provide information about the electronic structure of the absorbing atom in the material and the bonding properties with the neighboring atoms. The XANES region lies roughly 20–30 eV below and 40–50 eVabove the main absorption edge. While, 30–40 eV beyond the XANES region is calledNear Edge XAFS (NEXAFS), which has the strong multiple scattering tracks of the excited photoelectrons, the region beyond NEXAFS is called the Extended-XAFS (EXAFS).

The EXAFS region is due to the interference of the excited photoelectrons' incoming and outgoing wavefunctions after the scattering process from a nearest neighboring atom. The scattering mechanism is addressed by the EXAFS "chi" (χ) equation;

$$\chi=[\mu(E)-\mu_o(E)]/\Delta\mu_o \quad (1)$$

Here, μ denotes the absorbing coefficient. The chi signal can also be estimated via the parameters for the scattering of the photoelectrons, i.e., the EXAFS equation;

$$\chi(k)= \sum[(N_j\phi_j(k)\ \varepsilon x\pi(-2k^2\sigma_j^2))/(kP_j^2)]\sigma in[2kP_j+\delta_j(k)] \quad (2)$$

and "σ_j^2 " is the mean-square disorder with the neighboring atom distances. Here, "N" is the coordination number of the neighboring atom, "f (k)" is the scattering amplitude, "$\delta_j(k)$" is the scattering phase shift, "R" is the distance of the neighboring atom As the scattering data is related to the photoelectrons' interactions among the atoms and it is indirectly gives information about the mean free path which means the average distance travelled by the photoelectron, i.e. $k\sim1/\lambda$. In the absorption process, the photoelectron is created with the transferred excess kinetic energy by the photon-electron interaction mechanism. If an incident photon excites a core electron with an energy above the bond energy, the rest of the energy is used as the kinetic energy by the photoelectron to free itself from its source atom. The kinetic energy has a high reduction due to the interstitial potentials when a different type of atoms is in the neighborhood. Such kinds of materials reveals roughness in the interstitial potential where photoelectrons lost much of their kinetic energy and shorten their mean free paths. The mean free path of the photoelectron also highlights the potential distribution in the material that has an important influence on the conductivity of the material via the free electrons. In a material, the lowest product of "$\rho\times\lambda$" is related to the highest conductivity on a metal wire [5].

Materials are classified as conductors, semiconductors, or insulators according to their electric charge or heat transfer capabilities. Most of the metals are conductive and the least conductive materials are called insulators such as wood, plastics, and ceramics. Best conductive metals are known as silver, copper, gold, aluminum, rhodium, etc.. There are different techniques to determine the conductivity or resistance of the metals, like 4– point probe, electrochemical analysis, Hall effect, etc..The electrical conductivity behavior of the materials is directly related to the mean free path of the free electrons. In a material, free electrons travel in the interstitial potential which obtained jointly by the atoms in the material. So from the point of view, data collected with the XAFS technique can also be used to estimate the electrical properties of the materials.

To study the single crystalline metals is useful to find out such a relation to avoid the effects of the impurities and the defects that can naturally occur in the materials. Besides, the yields of a substitution process can also provide data to enlighten the interplays between the host and the substituted atom in a crystal. In this study, boron atoms are substituted in the iron coordination to reveal its influence on bonding and chemical environment via the electronic properties. In this study, 10% boron substituted $CuFeO_2$ oxide material was studied theoretically for its electronic and crystal structure properties.

2. Materials and Method

The calculations for the study are performed by the FEFF 8.2 code, which is a space multiple scattering approach [8-10]. For the calculation of the XAFS analysis, data were produced from the Fe K-edge of the $CuFeO_2$ and $CuFe_{1-x}B_xO_2$ boron substituted oxide. For the calculations, input files were generated by the TkAtoms code [11]. An iron atom in the input file was selected as the source atom, i.e. the photoelectron emitter.The input file was generated for 15 A˚ thick $CuFeO_2$cluster containing 656 atoms (Cu, Fe, and O) and 656 atoms (Cu ,Fe, B, and O), where a Fe atom was chosen as the source atom. For the calculations, XRD data was created via the MAUD software which is a diffraction/reflectivity analysis code [12].

3. Results and Discussion

Calculated x-ray diffraction pattern data is given in figure 1 as a comparison of the boron substituted and the pure $CuFeO_2$ oxide. The bold sketched XRD pattern has been taken from a real sample of us (that's the reason for the noisy data) and the pattern in red is calculated by the MAUD software with 10% boron substitutions in iron coordinations in the $CuFeO_2$ cluster.

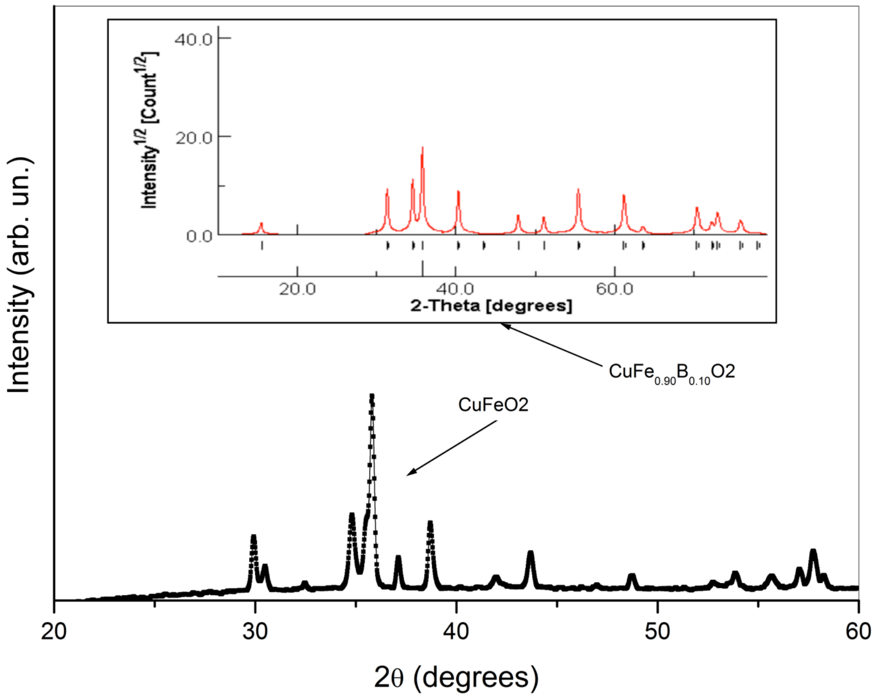

Fig. 1. Comparison for the XRD patterns of $CuFeO_2$ and 10% boron substituted $CuFeO_2$.

With the boron substitution in the iron coordination, a change in the XRD pattern peak positions was observed. No extra powerful peak formation has been observed and this means that boron atoms sit in Fe locations and preserved the crystal structure properties. To probe the influence of boron substitution on the electronic structure of its neighbors, on the iron, or on the crystal structure properties, X-ray absorption Fine Structure (XAFS) Spectroscopy study is the best choice. In Figure 2, calculated Fe K-edge XAFS spectra of the $CuFeO_2$ and 10% boron substituted $CuFeO_2$ material are given in comparison.

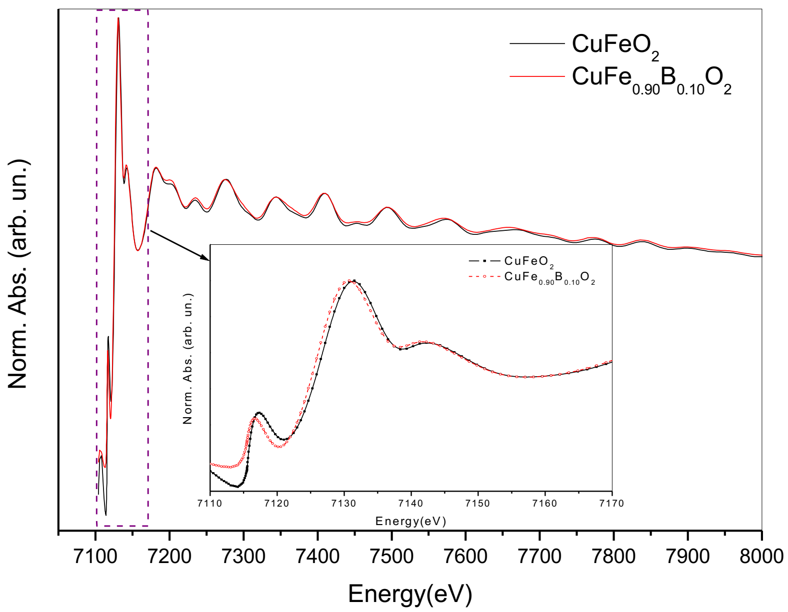

Fig. 2. Fe K-edge XAFS spectral comparison for the $CuFeO_2$ and 10% boron substituted $CuFeO_2$.

A high agreement in the XAFS spectra of the materials is observed in fig.2. The symmetry of both absorption spectral features has confirmed the calculated XRD patterns. However, a slight energy shift (0.7 eV) to the lower energy side in the boron substituted sample highlights the change in the oxidation state of the iron electronic structure. The absorption peak of the pure $CuFeO_2$ oxide has a maximum at 7131.4 eV and boron substituted material has the maximum at 7130.7 eV. The inset in the figure is also given to guide for the details. Fe K-edge spectra are a result of the 1s electron transition to unoccupied 4p levels in an excitation process. Actually, 3d levels are also unoccupied, but due to the quantum selection rules, electronic transitions of s→d is dipole forbidden. Thus, 1s electrons can make transitions to the 4p level which is located above the 3d level as the main route. However, with a hybridization via O 2p-Fe 3d levels, quadrupolar transitions may also occur weakly. The weak peak feature just below the main edge is a result of the quadrupolar interaction and this part is called the pre-edge peak. The pre-edge peak addresses a powerful Fe-O hybridization via the strong coupling between the outer shell electrons of the neighboring iron and oxygen atoms.

Boron has the same ionic value (3+) as ionic iron. However, the ionic radii of boron and iron have highly different values as; 0.023 nm and 0.060 nm, respectively. Despite the confirmation of the boron locations in the iron coordination by the XRD patterns and XAFS spectra, huge difference in the ionic radii of the atoms in the substitution processes should be a problem for boron to sit in the iron coordination. The effect of the boron substitution in the crystal order of the $CuFeO_2$ material can be best analyzed by the scattering amplitude which can be extracted from the Extended XAFS (EXAFS) part via the given equation (1). The scattering intensity graph is given in figure 3.

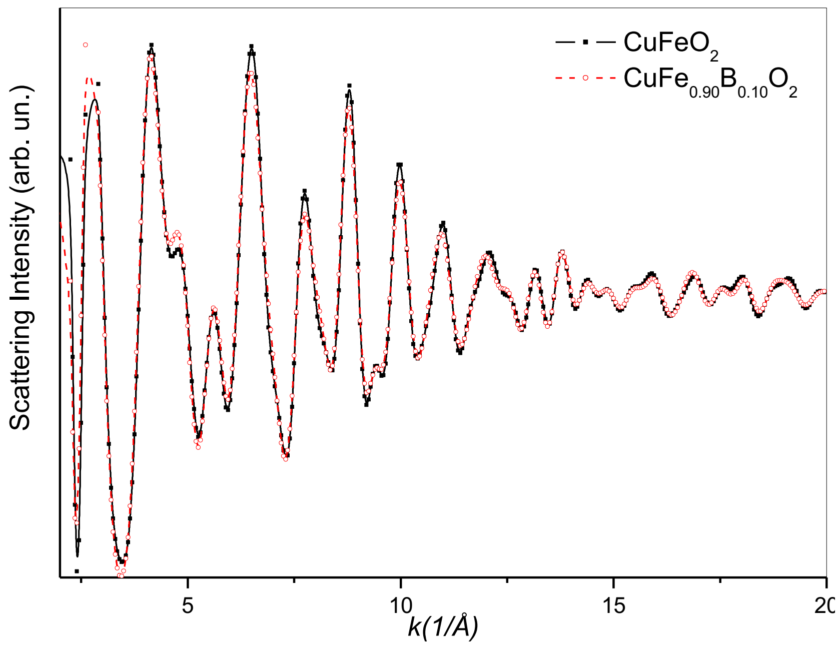

Fig. 3. EXAFS scattering intensity comparison for the $CuFeO_2$ and 10% boron substituted $CuFeO_2$.

In figure 3, high agreement with the peak structures and also the high symmetry in the spectra also confirms the remaining crystal structure in the material, even boron substitution.

However, weak decays at some scattering intensities highlight the light atoms' presence in the crystal, i.e., Boron. When a substitution occurs in a material, the interstitial potential among the atoms in the material causes fluctuations for the photoelectrons where it travels. The fluctuations are due to the change in the merits of the potential of the neighboring atoms. When the substitution is taken into account for the light atoms, if it sits in the coordination of another atom, like here, the photoelectrons' kinetic energy decay is lesser than before. For heavier atoms' substitution is subject to a study, then new interstitial potential becomes fatal for the photoelectrons due to the increase in the potential borders, which are treated as barriers. The Fourier transform (FT) of the scattering intensity yields the Radial Distribution Function (RDF) of the atoms in the crystal. The RDF gives the atomic locations and distances of the atoms which are located mainly in the first and the second-row vicinity of the source atom, which is located in the origin on the 1D axis. In figure 4, the RDF of the pure $CuFeO_2$ material is given in comparison with the boron substitute $CuFeO_2$ material.

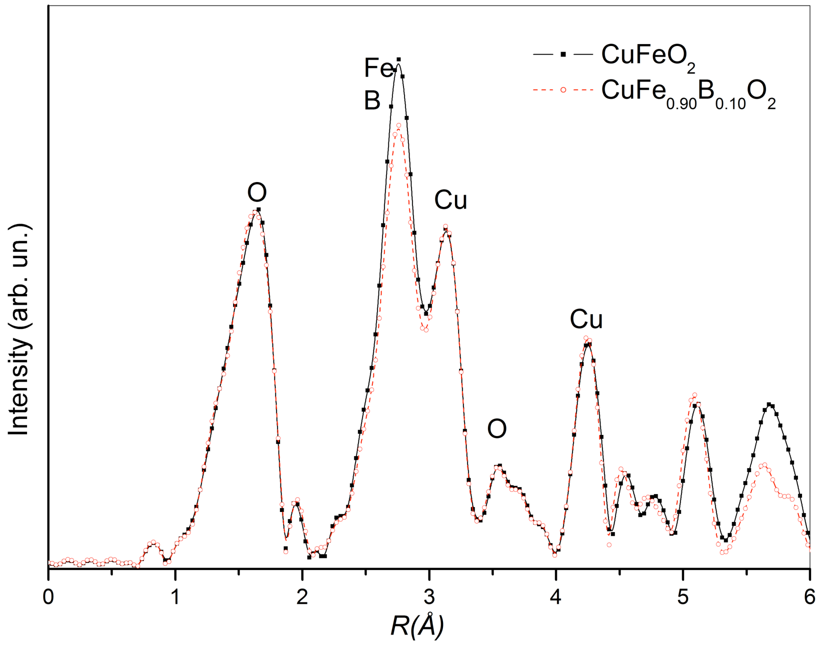

Fig. 4. Radial Distribution Function intensity of the $CuFeO_2$ and 10% boron substituted $CuFeO_2$.

According to figure 4, the boron sitting peaks are apparent and no need for any extra analysis to find out the boron locations. Analysis results of figure 4, the atomic distances from the source Fe atom which is sitting at the origin are: O atoms sit at 1.98 Å distance from an iron atom, Fe atoms sit at 3.01 Å distance and one of them is Boron. The third nearest neighbor is determined as the copper (Cu) atom which is located at a 3.34 Å distance.

4. Conclusion

In this study, boron atoms were substituted in the Fe coordinations. Due to the high difference in the ionic radii of the host and substituted atoms, different crystal structure formation was expected. However, calculations showed that boron atoms tend to locate in Fe coordination and prefer to the part of the host crystal and bond with the oxygen atoms strongly which are in its neighborhood. The presence of the light boron atoms was determined to weaken the scattering intensities which cause a longer mean free path for the photoelectrons. The longer mean free path means lower interstitial potential and hence it means a better conductivity of the material, according to the equation that gives the conductivity; i.e.,$\rho\times\lambda$.

5. References

[1] Ozkendir, O.M., The electronic structure study of Fe L3 edge in CuFeO2, *J. Optoelectron. Adv. Mater. Rapid Commun*, 3, 586-591, 2009.

[2] Eerenstein, W., Mathur, N.D., Scott, J.F., Multiferroic and magnetoelectric materials, *Nature,* 442, 759, 2006.

[3] Ozkendir, O.M., Boron Activity in Metal Containing Materials, *Advanced Journal of Chemistry, Section B: Natural Products and Medical Chemistry*, 2 (2), 48-54, 2020.

[4] Ozkendir, O.M., Yuzer, A., Influence of Sm-substitution on the crystal and electronic structure of the FeBO3 oxide, *Journal of Optoelectronics and Advanced Materials*, 20(3-4), 201-207, 2018.

[5] Ozkendir, O.M., Crystal and Electronic Study of Neodymium-Substituted CuFeO2 Oxide, *Metallurgical and Materials Transactions A*, 47(6), 2906-2913, 2016.

[6] Thole, B.T., Carra, P., Sette, F., Van der Laan, G., *X-ray circular dichroism as a probe of orbital magnetization,* Phys. *Rev. Lett.*, 68, 1943, 1992.

[7] Gall, D., Electron mean free path in elemental metals, *Journal of Applied Physics,* 119, 085101, 2016.

[8] Ozkendir, O.M., Crystal and Electronic Study of Neodymium-Substituted CuFeO2 Oxide, *Metallurgical Materials and Metals Transaction A,* 47A, 2906-2913, 2016.

[9] Ozkendir, O.M., Structural and Magnetic Study of CuxFeCr1−xO2 Oxides Under High External Magnetic Fields, *J. Electron. Mater.,* 42(6), 1055–1062, 2013.

[11] Ankudinov, A.L., Ravel, B., Rehr, J.J., Conradson, S.D., Relativistic calculations of spin-dependent x-ray-absorption spectra, *Phys. Rev. B,* 56, R1712, 1997.

[12]Ravel, B., ATOMS: crystallography for the X-ray absorption spectroscopist, *J. Synchrotron Radiat.*, 8(2), 314, 2001.

[13] Lutterotti, L., Chateigner, D., Ferrari, S., Ricote, J., Texture, residual stress and structural analysis of thin films using a combined X-ray analysis, *Thin Solid Films*, 450, 34-41, 2004.

International Journal of Engineering & Applied Sciences (IJEAS)
Vol. 13, Issue 1 (2021) 17-35
http://dx.doi.org/10.24107/ijeas.865695
Int J Eng Appl Sci 13(1) (2021) 17-35

Buckling Analysis of Rectangular Beams Having Ceramic Liners at Its Top and Bottom Surfaces with the help of the Exact Transfer Matrix

Vebil Yıldırım

Dept. of Mechanical Engineering, University of Çukurova, Adana, Turkey
E-mail address: vebil@cu.edu.tr

ORCID number of the author:
0000-0001-9955-8423

Received date: 20.01.2021
Accepted date: 31.03.2021

Abstract

In this study the elastic buckling behavior of beams with rectangular cross section is studied analytically. It is assumed that both the top and bottom surfaces of the beam are ceramic coated. The aluminum (Al) is chosen as a core material while the aluminum-oxide (Al_2O_3) is preferred as a liner (face) material. The transfer matrix method based on the Euler-Bernoulli beam theory is employed in the analysis. The exact transfer matrix in terms of equivalent bending stiffness is presented together with the exact buckling equations for hinged-hinged, clamped-hinged, clamped-free, and finally clamped-clamped boundary conditions. After verifying the results for beams without liners, dimensionless buckling loads of the beam with ceramic liners are numerically computed for each boundary condition. The effect of the thickness of the ceramic liner on the buckling loads is also investigated. It is found that a ceramic liner enhances noticeably the buckling loads. As an additional study those effects are also examined for the ratios of elasticity modulus of face material to core material in a wide range.

Keywords: Exact buckling, Euler-Bernoulli, transfer matrix, stability, sandwich beam, critical buckling loads

1. Introduction

Buckling of columns being a physical phenomenon is a matter of significance in the design of structural elements. Underestimation of this phenomenon may lead to disastrous results.

Buckling occurs in beams subjected to compressive loads. The longer and more slender the column is, the lower the safe compressive stress that it can stand. The maximum load at which the column tends to have lateral displacement or tends to buckle is known as critical buckling or crippling load. Therefore in the design of columns, determination of the critical buckling loads becomes an inevitable stage.

Research into buckling of columns dates back to late 1700s with Euler's study [1]. Greenhill's [2], Dinnik's [3], and Timoshenko and Gere's [4] studies are some subsequent fundamental works to Euler's [1] study in the related realm. Numerous analytical and numerical works on the stability of columns were conducted after those pioneers [5-42]. From those methods which can be used to determine the elastic critical buckling load may be summarized as the differential equation solution method [1-11], energy methods [12-16], the finite element method [17-22], the finite difference method [23], the modified slope deflection method [24], the effective-thickness concept [25], the multi-segment integration technique [23], the variational iteration method [26-28], the homotopy perturbation method [28-33], Adomian decomposition method [28, 34], the transfer matrix method [35-39], the stiffness matrix method [39], the fictitious load method [40], the modified vibration modes [41] and much more [42-46]. In the solution of more complex problems, some of the solution methods mentioned above may also be used in a combined manner.

The governing buckling differential equation may be obtained based on the either beam or elasticity [9-11] theories. The beam theories allow to solve much more complex problems for a beam or a system of beams. The governing equation in differential form may then be solved by using exact or approximate solution techniques. As may be guessed it is possible to obtain exact solutions for relatively simple problems.

As is known, the gain of strain energy in the elements is less than the potential energy of the loads which are lower than the elastic critical load. If the change of these two energies is zero then the structure will not resist any disturbance. This stage at which the stiffness of the structure is zero is defined as a critical instability condition in the energy methods.

In the finite element method, in which the structure is subdivided into a series of fairly short elements, buckling is considered by adding a geometrical stiffness matrix to the element equations. The resulting eigenvalue problem is then solved by applying several techniques such as vector iteration methods (inverse iteration, forward iteration, and Rayleigh quotient iteration), transformation methods (Jacobi method, the subspace iteration method).

The transfer matrix method is one of the methods to the solution of initial value problem (IVP). Many problems from the simplest one to the complex ones may be solved with the help of this technique. The governing equations in canonical form, which is a relationship between the section quantities and their first derivatives, may be obtained from the either beam or elasticity theories. In the method, determination of the elements of the transfer matrix is crucial. The overall transfer matrix, which is obtained from the solution of a set of differential equation having either constant or variable coefficients, relates the section quantities at the initial point and at any point on the beam axis. The accuracy of the solution directly depends on the accuracy of the overall transfer matrix to be derived. It is possible to obtain some closed form solutions for the governing equation with constant coefficients. Otherwise, in case of existence of variable coefficients, the transfer matrix should be determined numerically. Contrary to the finite elements method, orders of the resulting matrices are independent from the number of elements to be considered. Therefore it is possible to construct easy-to-use algorithms with the transfer matrix method which are highly accurate and computationally efficient.

A sandwich structure usually consists of two relatively thin, stiff and strong faces separated by a relatively thick lightweight core. The main purpose of a sandwich structure is to achieve a stiff and simultaneously light component. That is higher stiffness and strength can be achieved by sandwich structures without increasing the weight dramatically. Sandwich constructions are also used for the aim of thermal insulation, corrosion insulation, vibration/noise damping, and water ingress prevention. Buckling phenomenon is a crucial task to be considered in the analysis of such structures [47-53]. This may be conducted by using any of the methods mentioned above. Recently, Sayyad and Ghugal [54] reviewed bending buckling, and free vibration of laminated composite and sandwich beams up to 2017s.

As is well known, Euler-Bernoulli theory is a simple beam theory by which one may get exact results which are reasonable for long and slender structural members. The theory offers overestimate buckling loads for relatively short columns. In other words, Euler buckling loads are independent from the ratio of the total length of the beam to the width of the section. In the present study, the effect of the existence of the liners on the buckling loads of a rectangular beam is intended for an examination with the help of the transfer matrix method. As a basic work, Euler-Bernoulli beam theory is employed to achieve fast and reasonable buckling loads.

2. Theory

Consider a beam subjected to an axial compressive load N whose critical value called the critical buckling load satisfies the following fourth order Euler-Bernoulli differential equation in terms of transverse displacement, w [1-8].

$$\frac{d^4w}{dx^4} + \frac{N}{EI}\frac{d^2w}{dx^2} = 0 \tag{1}$$

Where, x is the coordinate along the beam axis, E is Young's modulus and I is the area moment of inertia about y axis (Fig. 1). Derivation of Eq. (1) may be found in References [1-8]. The general solution of the foregoing well-known ODE is

$$w(x) = Acos\alpha x + Bsin\alpha x + Cx + D \tag{2}$$

where

$$\alpha = \sqrt{\frac{N}{EI}} \tag{3}$$

Solution to Eq. (2) is used with the following classical boundary conditions to determine the critical buckling loads of the beam. The boundary conditions for hinged ends are,

$$w = 0, \ w'' = 0 \tag{4}$$

for clamped ends are,

$$w = 0, \quad w' = 0 \tag{5}$$

and for free ends are

$$w''' = 0, \qquad w^{IV} = 0 \tag{6}$$

The number of the problems to be directly solved by Eq. (1) is limited. To consider a wider range applications of beams with initial axial force, the transfer matrix method is preferred in the present study. As stated in the introduction, one need to put the single fourth order differential equation given in Eq. (1) into a set of four differential equations of first order to be able to apply the transfer matrix method . The equations governing the elastic buckling behavior of an Euler-Bernoulli beam is given in canonical form as follows [5]

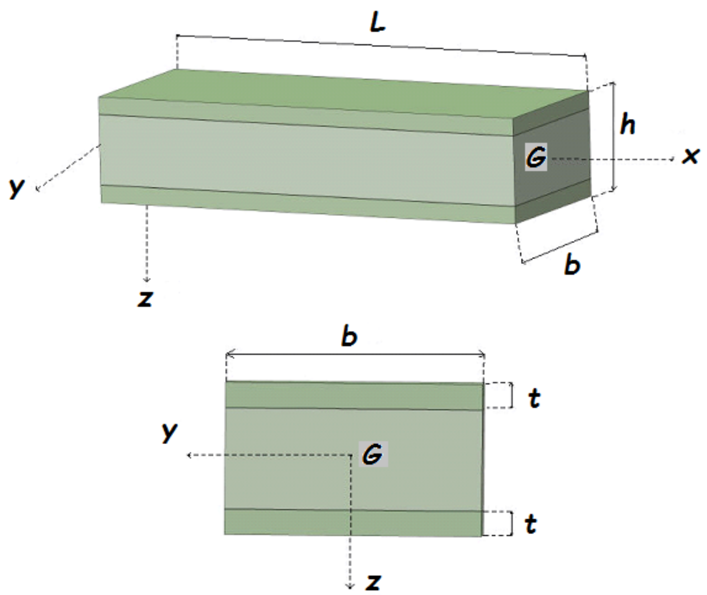

Fig. 1. The beam geometry and the coordinates

$$\frac{dw}{dx} = \theta \tag{7a}$$

$$\frac{d\theta}{dx} = -\frac{M}{EI} \tag{7b}$$

$$\frac{dM}{dx} = T + N\theta \tag{7c}$$

$$\frac{dT}{dx} = 0 \tag{7d}$$

where, w is still the transverse displacement, θ is the rotation, M is the bending moment, T is the shear force, N is the axial compressive constant initial force. Equation (7), which is identically equal to Eq. (1), may be written in a compact form as

$$\boldsymbol{S}'(x) = \boldsymbol{D}\,\boldsymbol{S}(x) \tag{8}$$

where the state vector which comprises the section quantities is defined by

$$\boldsymbol{S}(x) = \begin{bmatrix} w(x) \\ \theta(x) \\ M(x) \\ T(x) \end{bmatrix} \tag{9}$$

and the differential transfer matrix is

$$\boldsymbol{D} = \begin{bmatrix} 0 & 1 & 0 & 0 \\ 0 & 0 & \dfrac{-1}{EI} & 0 \\ 0 & N & 0 & 1 \\ 0 & 0 & 0 & 0 \end{bmatrix} \tag{10}$$

There are a few ways for the determination of the elements of the transfer matrix, $\boldsymbol{F}$ [5]. If the elements of the differential transfer matrix are constants as in beams having unchanged section and material properties along the beam axis, it is possible to get an exact solution for the element transfer matrix as in the present study.

Recalling that the element transfer matrix satisfy the similar differential equation for the state vector as in Eq. (8) the following may be written [5]

$$\boldsymbol{F}'(x) = \boldsymbol{D}\,\boldsymbol{F}(x) \tag{11}$$

Solution of Eq. (11) with the initial conditions

$$\boldsymbol{F}(x = 0) = \boldsymbol{I} \tag{12}$$

gives us the exact element transfer matrix in the form of a matrix exponential.

$$\boldsymbol{F}(x) = e^{x\boldsymbol{D}} = 1 + x\boldsymbol{D} + \frac{x^2}{2!}\boldsymbol{D}^2 + \frac{x^3}{3!}\boldsymbol{D}^3 + \frac{x^4}{4!}\boldsymbol{D}^4 + \frac{x^5}{5!}\boldsymbol{D}^5 + \frac{x^6}{6!}\boldsymbol{D}^6 + \cdots \tag{13}$$

In the above, $\boldsymbol{I}$ refers the unit matrix. In Eq. (13) the higher powers of the differential matrix which are equal or greater than four may be written in terms of the differential transfer matrices having smaller powers of up to three. To this end one may resort to Cayley-Hamilton theorem which states that every square matrix satisfies its own characteristic equation, $|\boldsymbol{D}\text{-}\mu\boldsymbol{I}| = 0$. Using Eq. (13) together with Cayley Hamilton theorem, Eq. (13) takes the following form in terms of up to the third powers of the differential transfer matrix [5].

$$\begin{aligned} \boldsymbol{F}(x) = 1 + x\boldsymbol{D} &+ \left(\frac{x^2}{2!} - \frac{x^4}{4!}\alpha^2 + \frac{x^6}{6!}\alpha^4 - \frac{x^8}{8!}\alpha^6 + \frac{x^{10}}{10!}\alpha^8 - \cdots\right)\boldsymbol{D}^2 \\ &+ \left(\frac{x^3}{3!} - \frac{x^5}{5!}\alpha^2 + \frac{x^7}{7!}\alpha^4 - \frac{x^9}{9!}\alpha^6 + \cdots\right)\boldsymbol{D}^3 \end{aligned} \tag{14}$$

The coefficients of the differential transfer matrix, which are in series form, correspond explicitly to the following functions

$$\boldsymbol{F}(x) = 1 + x\boldsymbol{D} + \frac{1 - \cos(\alpha x)}{\alpha^2}\boldsymbol{D}^2 + \frac{\alpha x - \sin(\alpha x)}{\alpha^3}\boldsymbol{D}^3 \tag{15}$$

The explicit forms of the elements of the exact element transfer matrix in Eq. (15) are given below in terms of the equivalent bending stiffness.

$$F_{1,1} = F_{4,4} = 1$$

$$F_{2,1} = F_{3,1} = F_{4,1} = F_{4,2} = F_{4,3} = 0$$

$$F_{1,2} = F_{3,4} = \frac{sin\left(x\sqrt{\frac{N}{E_{eq}I}}\right)}{\sqrt{\frac{N}{E_{eq}I}}}$$

$$F_{1,3} = F_{2,4} = \frac{cos\left(x\sqrt{\frac{N}{E_{eq}I}}\right) - 1}{N}$$

$$F_{1,4} = \frac{\sqrt{E_{eq}I}\, sin\left(x\sqrt{\frac{N}{E_{eq}I}}\right)}{N^{\frac{3}{2}}} - \frac{x}{N} \tag{16}$$

$$F_{2,2} = F_{3,3} = cos\left(x\sqrt{\frac{N}{E_{eq}I}}\right)$$

$$F_{2,3} = -\frac{sin\left(x\sqrt{\frac{N}{E_{eq}I}}\right)}{\sqrt{N\, E_{eq}I}}$$

$$F_{3,2} = \sqrt{N\, E_{eq}I}\, sin\left(x\sqrt{\frac{N}{E_{eq}I}}\right)$$

The overall transfer matrix relates the state vectors at both ends of the beam as follows

$$\boldsymbol{S}(L) = \boldsymbol{F}(\boldsymbol{L})\, \boldsymbol{S}(0) \tag{17}$$

This equation may be expanded as

$$\begin{bmatrix} w \\ \theta \\ M \\ T \end{bmatrix}_{x=L} = \begin{bmatrix} F_{1,1} & F_{1,2} & F_{1,3} & F_{1,4} \\ F_{2,1} & F_{2,2} & F_{2,3} & F_{2,4} \\ F_{3,1} & F_{3,2} & F_{3,3} & F_{3,4} \\ F_{4,1} & F_{4,2} & F_{4,3} & F_{4,4} \end{bmatrix}_{x=L} \begin{bmatrix} w \\ \theta \\ M \\ T \end{bmatrix}_{x=0} \tag{18}$$

In the present study the following boundary conditions are implemented (Fig. 2) for hinged (pinned) ends as

$$w = 0, \quad M = 0 \tag{19}$$

for clamped ends as

$$w = 0, \quad \theta = 0 \tag{20}$$

and for free ends as

$$T = 0, \quad M = 0 \tag{21}$$

After implementing those boundary conditions in Eq. (13), the buckling equations are obtained as follows

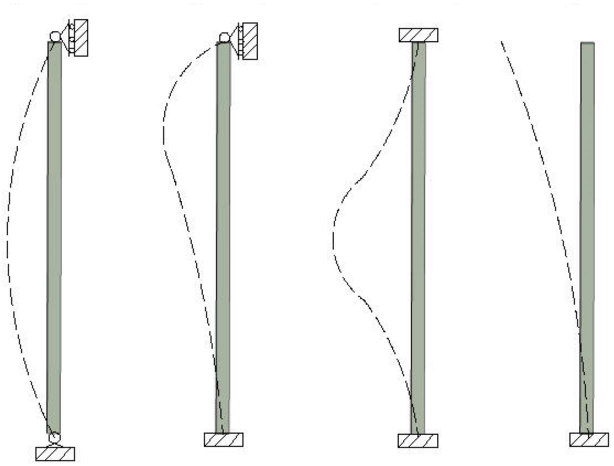

Fig. 2. Classical boundary conditions.

$$\begin{gathered}
|A|_{hinged-hinged} = \begin{vmatrix} F(L)_{1,2} & F(L)_{1,4} \\ F(L)_{3,2} & F(L)_{3,4} \end{vmatrix} = 0 \\
|A|_{clamped-free} = \begin{vmatrix} F(L)_{3,3} & F(L)_{3,4} \\ F(L)_{4,3} & F(L)_{4,4} \end{vmatrix} = 0 \\
|A|_{clamped-hinged} = \begin{vmatrix} F(L)_{1,3} & F(L)_{1,4} \\ F(L)_{3,3} & F(L)_{3,4} \end{vmatrix} = 0 \\
|A|_{clamped-clamped} = \begin{vmatrix} F(L)_{1,3} & F(L)_{1,4} \\ F(L)_{2,3} & F(L)_{2,4} \end{vmatrix} = 0
\end{gathered} \tag{22}$$

In the above the axial force making the corresponding determinants equal to zero is referred to as the critical buckling load, N_{cr}. These loads may be found by using the searching determinant method together with the bi-sectioned method, or other solution techniques.

The more compact forms of the determinants are given in Appendix.

3. Verifications of the results

For the sake of simplicity, the application of this method may be shown on the simple model of a column with uniform cross-section that is subjected to the axial compressive force N. The column is assumed to be made of a single isotropic and homogeneous material. The following dimensionless buckling load is defined to verify the results with the open literature

$$\beta = \frac{L^2}{EI} N \tag{23}$$

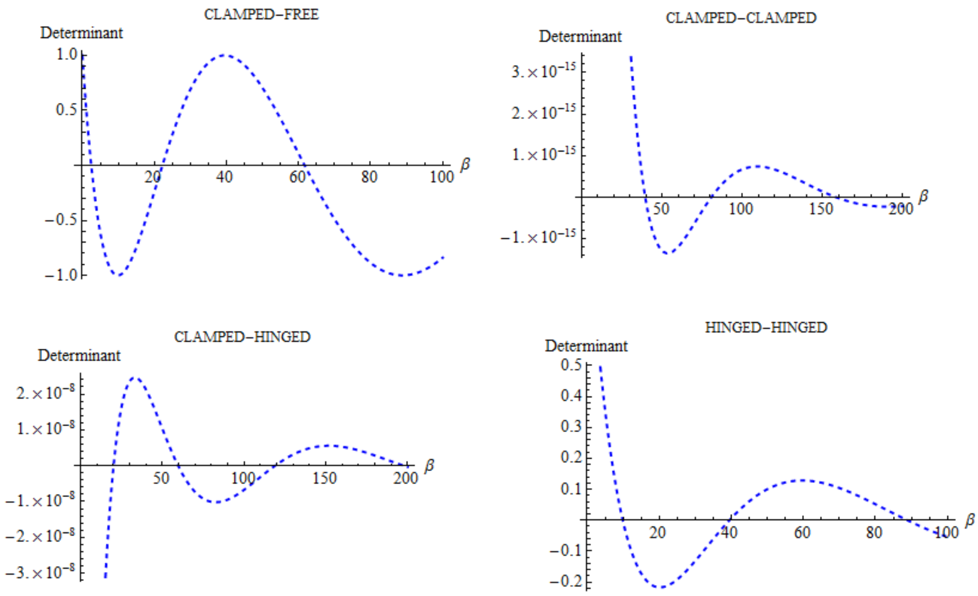

Fig. 3. Determinant-dimensionless frequency curves under classical boundary conditions.

Dimensionless buckling loads are listed in Table 1 in a comparative manner with the literature. A perfect harmony is observed among the results. The corresponding determinant curves are illustrated in Fig. 3. Further analytical verifications are given in Appendix A.

Table 1. Comparison of dimensionless critical Euler buckling loads of uniform columns without liners

	C–F	P–P	C–P	C–C
Present (Transfer matrix method)	2.4674	9.8696	20.1907	39.4784
Wang et al. [6] (Exact)	2.4674	9.8696	20.1907	39.4784
Saha and Banu [23] (Finite difference method)	--	9.8892	20.2044	39.786
Saha and Banu [23] (Multi-segment integration)	--	9.8728	20.1876	39.6408
Coşkun and Atay [27] (Variational iteration)	2.4674	9.8696	20.1908	39.4916
Eryılmaz et al. [33] (Homotopy analysis)	2.4674	9.8696	20.1907	39.4784

4. Effect of the liner thickness on the buckling loads

As stated before without increasing the weight dramatically, higher stiffness and strength can be achieved by sandwich structures with soft cores. Chakrabartia et al. [48] verified this for the buckling of laminated sandwich beams with soft cores. Although the proposed method may be applied to the laminated structures having anisotropic characteristics after a certain effort, both the face and core material are assumed to be isotropic and homogeneous in the present study for simplicity.

To study the effect of the total thickness of the bottom and top liners on the buckling loads, the following dimensionless quantity is defined.

$$\lambda = \frac{2t}{h} \tag{24}$$

where t is the thickness of a layer, h is the width of the rectangular section having length b (Fig. 1). The equivalent bending stiffness of the uniform section is derived as

$$E_{eq}I = \left((3\lambda^2 - \lambda^3 - 3\lambda + 1)E_1 + (-3\lambda^2 + \lambda^3 + 3\lambda)E_2\right)\frac{bh^3}{12} \tag{25}$$

In the above E_1 is Young's modulus of the core material while E_2 stands for the elasticity modulus of the liner material (face material). The dimensionless buckling load may now be defined in terms of Young's modulus of the core material.

$$\beta = \frac{L^2}{E_1 I}N \tag{26}$$

The material and geometrical properties used in the parametric study are: $E_1 = E_{core} = 70.0\ 10^9\ GPa\ (Al)$, $E_2 = E_{liner} = 393.0\ 10^9\ GPa\ (Al_2O_3)$, $b = 2h$; $L = 1.0\ m$; $L/h = 10$. Effect of the total thickness of the liners with respect to the height of the section is seen in Table 2 and Fig. 4 under all classical boundary conditions.

Table 2. Dimensionless critical buckling loads of uniform columns with liners

λ	C-F	P-P	C-P	C-C
0.0	2.4674	9.8696	20.1907	39.4784
0.01	2.80556	11.2222	22.9578	44.8889
0.02	3.13695	12.5478	25.6696	50.1912
0.05	4.09123	16.3649	33.4785	65.4597
0.1	5.55282	22.2113	45.4387	88.8451
0.2	8.02342	32.0937	65.6556	128.375
0.3	9.94754	39.7902	81.4007	159.161
0.4	11.3935	45.5739	93.2327	182.296
0.5	12.4295	49.7181	101.711	198.873
0.6	13.124	52.4961	107.394	209.985
0.7	13.5453	54.1812	110.841	216.725
0.8	13.7616	55.0464	112.611	220.186
0.9	13.8413	55.3652	113.263	221.461
1.0	13.8527	55.4108	113.357	221.643

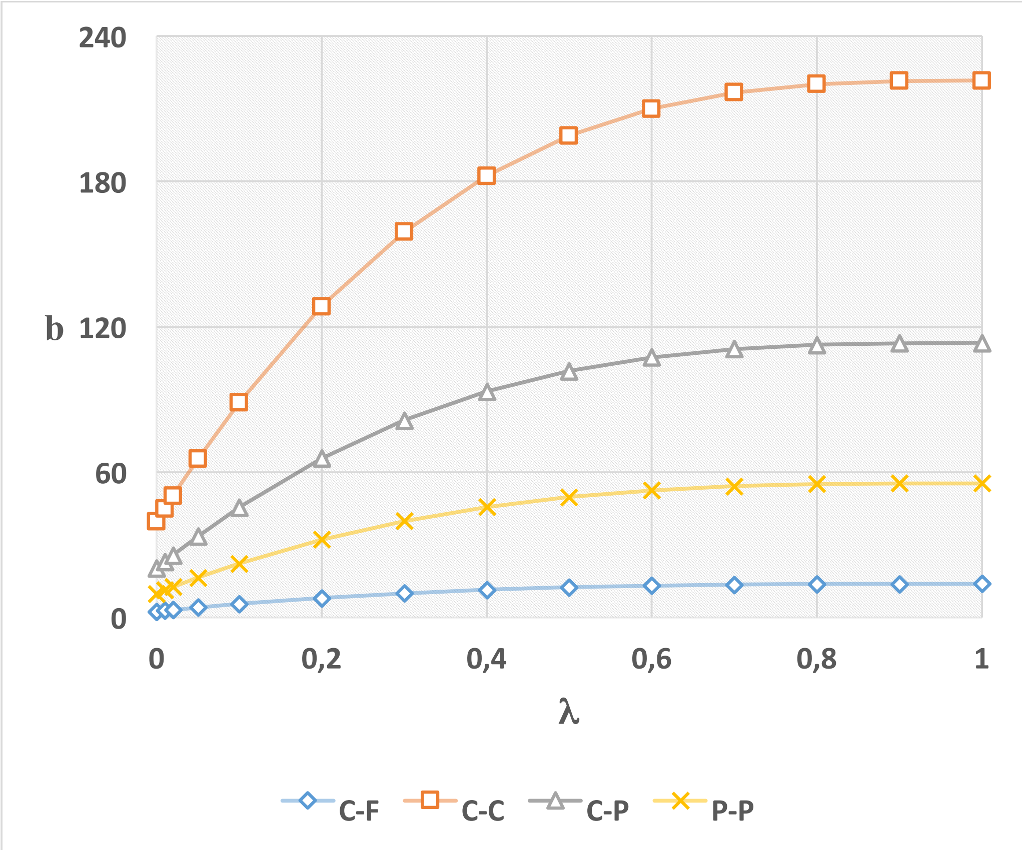

Fig. 4. Variation of the buckling loads with the total thickness of the liners

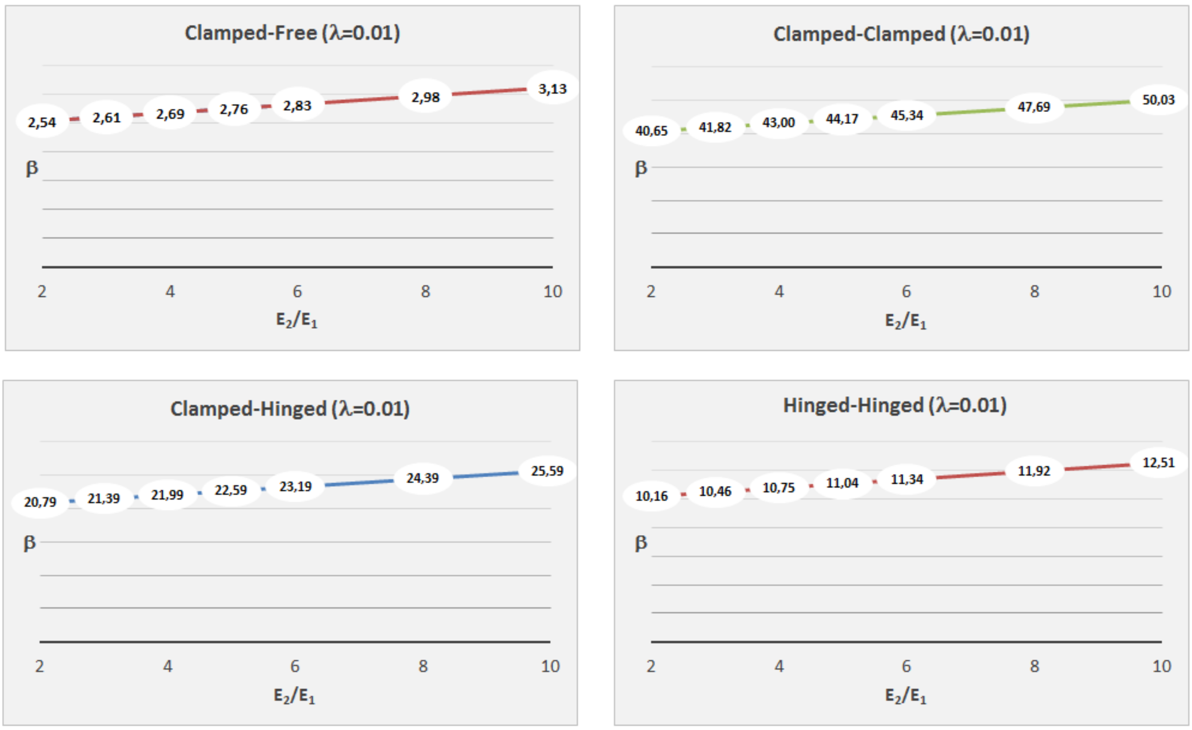

Fig. 5. Variation of the buckling loads with E_2/E_1 ratios and boundary conditions under all boundary conditions for $\lambda = 0.01$

From Table 2, it is revealed that for even very thin liners, $\lambda = 0.01$, the buckling load increases rapidly by over 10%. For $\lambda = 0.1$, the beam can withstand greater forces of around 22% more than the beam without liners. From Fig. 4, it may be concluded that the total thickness of the liners more than 50% is not feasible to enhance the buckling loads for the example considered.

To more generalize the problem for practical applications, let's consider a sandwich beam having a soft core and investigate the variation of the dimensionless buckling loads with E_2/E_1 ratios, liner thickness and boundary conditions ($b = 2h$; $L = 1.0\ m$; $L/h = 10$). The results are presented in Fig. 5, and Table 3.

Table 3. Variation of the buckling loads with the total thickness of the liners and E_2/E_1 ratios under all boundary conditions

	E_2 / E_1									
λ	2	3	5	8	10	2	3	5	8	10
	Clamped-Free					**Clamped-Clamped**				
0.0	2.4674	2.4674	2.4674	2.4674	2.4674	39.4784	39.4784	39.4784	39.4784	39.4784
0.01	2.54069	2.61397	2.76054	2.98039	3.12696	40.651	41.8235	44.1686	47.6863	50.0314
0.02	2.6125	2.75761	3.04781	3.48312	3.77333	41.8001	44.1217	48.765	55.7299	60.3732
0.05	2.81931	3.17123	3.87505	4.93079	5.63462	45.109	50.7396	62.0009	78.8927	90.1539
0.1	3.13607	3.80473	5.14206	7.14806	8.48539	50.1771	60.8757	82.273	114.369	135.766
0.2	3.67149	4.87558	7.28377	10.896	13.3042	58.7439	78.0094	116.54	174.337	212.868
0.3	4.08848	5.70957	8.95173	13.815	17.0571	65.4157	91.3531	143.228	221.04	272.914
0.4	4.40184	6.33629	10.2052	16.0085	19.8774	70.4295	101.381	163.283	256.136	318.038
0.5	4.62638	6.78535	11.1033	17.5802	21.8982	74.022	108.566	177.653	281.284	350.371
0.6	4.77689	7.08638	11.7054	18.6338	23.2528	76.4302	113.382	187.286	298.141	372.045
0.7	4.86818	7.26896	12.0705	19.2729	24.0744	77.8909	116.303	193.128	308.366	385.191
0.8	4.91506	7.36272	12.258	19.601	24.4964	78.641	117.804	196.129	313.617	391.942
0.9	4.93233	7.39727	12.3271	19.7219	24.6518	78.9174	118.356	197.234	315.551	394.429
1.0	4.9348	7.4022	12.337	19.7392	24.674	78.9568	118.435	197.392	315.827	394.784
	Clamped-Hinged					**Hinged-Hinged**				
0.0	20.1907	20.1907	20.1907	20.1907	20.1907	9.8696	9.8696	9.8696	9.8696	9.8696
0.01	20.7904	21.3901	22.5895	24.3885	25.5879	10.1627	10.4559	11.0422	11.9216	12.5078
0.02	21.3781	22.5655	24.9402	28.5024	30.8771	10.45	11.0304	12.1913	13.9325	15.0933
0.05	23.0704	25.9501	31.7095	40.3486	46.1081	11.2773	12.6849	15.5002	19.7232	22.5385
0.1	25.6624	31.1341	42.0775	58.4925	69.4359	12.5443	15.2189	20.5683	28.5922	33.9416
0.2	30.0438	39.8969	59.603	89.1623	108.868	14.686	19.5023	29.1351	43.5842	53.2169
0.3	33.456	46.7213	73.252	113.048	139.579	16.3539	22.8383	35.8069	55.2599	68.2286
0.4	36.0203	51.8498	83.5089	130.997	162.657	17.6074	25.3451	40.8207	64.034	79.5095
0.5	37.8576	55.5245	90.8583	143.859	179.193	18.5055	27.1414	44.4132	70.3209	87.5927
0.6	39.0893	57.9878	95.7848	152.48	190.277	19.1076	28.3455	46.8214	74.5353	93.0112
0.7	39.8363	59.4819	98.773	157.71	197.001	19.4727	29.0759	48.2821	77.0915	96.2977
0.8	40.2199	60.2491	100.308	160.395	200.454	19.6603	29.4509	49.0322	78.4041	97.9854
0.9	40.3613	60.5318	100.873	161.384	201.726	19.7293	29.5891	49.3085	78.8877	98.6072
1.0	40.3815	60.5722	100.954	161.526	201.907	19.7392	29.6088	49.348	78.9568	98.696

As stated above, if the aluminum is a core material and the aluminum-oxide is a face material, the buckling load increases rapidly over 10% for $\lambda = 0.01$. This contribution is linearly changed with the E_2/E_1 ratios for the same ratio of λ (Fig. 5). For instance, under all boundary conditions and for λ=0.01, the buckling loads increase by 3% if $E_2/E_1 = 2$, by 12% if $E_2/E_1 = 5$, and by 27% if $E_2/E_1 = 10$.

For $\lambda=0.1$, the improved buckling load reaches about 1.3 times the buckling load of the beam made from only the core material if E_2/E_1 =2. It is around 2 times of the buckling load without liners if E_2/E_1 =5, and is approximately 3.5 times that load if E_2/E_1 =10.

7. Conclusions

In the present study the effect of the thickness of liners on the critical buckling loads of a beam having uniform rectangular cross-section is investigated based on the Euler-Bernoulli beam theory under several boundary conditions. Real-life materials together with hypothetical ones are used in the examples.

The transfer matrix method is chosen for the solution procedure due to its effective, economical, and accurate results together with its wider applications in the engineering realm. The element transfer matrix is obtained analytically by solving a set of four differential equations of first order. The effective bending rigidity is used in the determination of the elements of the exact element transfer matrix. This approach is reasonably suitable for especially industrial applications

As a first stage of the present work, the critical buckling loads are obtained for a uniform beam without liners and compared with the literature. Perfect agreement is observed among the buckling loads.

In the next stage, a rectangular sectioned beam is handled to observe the variation of the effect of the liner thickness on the buckling loads. The aluminum (Al) is used for a core material and the aluminum-oxide (Al_2O_3) for a liner (face) material. It is discovered that for even very thin liners, $\lambda = 0.01$, the buckling load increases rapidly by over 10%. For $\lambda = 0.1$, the beam can tolerate greater buckling loads of around 22% more than the buckling loads of the beam without liners.

In the last stage, a generalized parametric study is conducted for various ratios of Young's modulus of the core material to the face material from 2 to 10. It is observed that under all boundary conditions and for λ=0.01, the buckling loads increase by 3% if E_2/E_1 =2, by 27% if E_2/E_1 =10. For λ=0.1, the improved buckling load reaches about 1.3 times the buckling load of the beam made from only the core material if E_2/E_1 2, and is around 3.5 times that load if E_2/E_1 =10.

It is chiefly concluded that the thickness of the liner strongly affects the buckling loads. However the ratio of the total thickness of the liners to the total width of the section is not feasible if it reaches over 50%.

It is also revealed that the transfer matrix method leading to exact solutions may be used effectively in the analysis of elastic stability problems of such structures. The method offered here may also be applied to the multi-spanned beams, beam systems having different bending rigidities under classical/non-classical boundary conditions.

Notations

α Dimensionless buckling parameter
β Dimensionless buckling load
θ Rotation about y-axis
$\boldsymbol{A}$ Characteristic buckling coefficient matrix
b Base length of rectangular cross section of the beam
$\boldsymbol{D}$ Differential transfer matrix
E Elasticity modulus of the beam material
$E_{eq}I$ Equivalent bending stiffness
$\boldsymbol{F}$ Transfer matrix
h Width of rectangular section
I Area moment of inertia about y-axis
$\boldsymbol{I}$ Unit matrix
L Length of the beam
M Bending moment about y-axis
N Axial compressive load
N_{cr} Critical buckling load
$\boldsymbol{S}$ State vector
t Thickness of one of liners
T Shearing force
w Transverse displacement along z-axis
x Position coordinate along the beam axis

References

[1] Euler, L., Die altitudine colomnarum sub proprio pondere corruentium, *Acta Acad Petropol,* 1778.
[2] Greenhill, A.G., Determination of the greatest height consistent with stability that a vertical pole on mast can be made and of the greatest height to which a tree of given proportions can grow in, *Proceedings of the Cambridge Philosophical Society*, IV, 1883.
[3] Dinnik, A.N., Design of columns of varying cross-section, *Transactions of the ASME*, 51, 1929.
[4] Timoshenko S.P., Gere J.M., *Theory of Elastic Stability*, McGraw-Hill Companies, 2nd edition, New York; 1961.
[5] İnan, M., *The Method of Initial Values and the Carry-Over Matrix in Elastomechanics*, ODTÜ Publication, No: 20; 1968.
[6] Chen W.F., Lui E.M., *Structural Stability, Theory and Implementation*, Elsevier, New York; 1987.
[7] Wang C.M., Wang C.Y., Reddy J.N., *Exact Solutions for Buckling of Structural Members*, CRC Press, Boca Raton, Fla, USA; 2005.
[8] Yoo C.H., Lee S.C., *Stability of Structures - Principles and Applications*, Butterworth Heinemann, New York; 2011.
[9] Smith, C.S., Application of folded plate analysis to bending, buckling and vibration of multilayer orthotropic sandwich beams and panels, *Comput Struct*, 22(3), 491–497, 1986.
[10] Kardomateas, G.A., Three dimensional elasticity solution for the buckling of transversely isotropic rods: the Euler load revisited, *ASME J Appl Mech*, 62, 346–55, 1995.

[11] D'Ottavio, M., Polit, O., Ji, W., Waas, A.M., Benchmark solutions and assessment of variable kinematics models for global and local buckling of sandwich struts, *Compos Struct*, 156, 125–134,2016.
[12] Pi, Y.L., Trahair, N.S., Rajasekaran, S., Energy equation for beam lateral buckling, *Journal of Structural Engineering, ASCE*, 118(6), 1462-1479, 1992.
[13] Wang, C.M., Wang, L., Ang, K.K., Beam-buckling analysis via automated Rayleigh-Ritz method, Journal of Structural Engineering, ASCE, 120(1), 200-211, 1994.
[14] Tong, G., Zhang, L., A general theory for the flexural-torsional buckling of thin-walled members I: Energy method, *Advances in Structural Engineering*, 6(4), 293-298, 2003.
[15] Zdravković, N., Gašić, K.M., Savković, K.M., Energy method in efficient estimation of elastic buckling critical load of axially loaded three-segment stepped column, *FME Transactions*, 41(3), 222-229, 2013.
[16] Kundu, B., Ganguli, R., Analysis of weak solution of Euler–Bernoulli beam with axial force, *Applied Mathematics and Computation,* 298, 247-260, 2017.
[17] Barsoum, R.S., Gallagher, R.H., Finite element analysis of torsional and torsional-flexural stability problems, *Int J Num Meth Engng,* 2, 335-352, 1970.
[18] Kabaila, A.P., Fraeijs de Veubeke, B., Stability analysis by finite elements, *Air Force Flight Dynamics Laboratory, Tech. Report AFFDL-TR-70-35*, 1970.
[19] Thomas, J.M., A finite element approach to the structural instability of beam columns, frames and arches, *NASA TN D-5782*, 1970.
[20] He, B., Zhang, H., Stability analysis of slope based on finite element method, *I J Engineering and Manufacturing, MECS,* 3, 70-74, 2012.
[21] Li, J.J., Li, G.Q., Buckling analysis of tapered lattice columns using a generalized finite element, *Commun Numer Meth Engng,* 20(6), 479–488, 2004.
[22] Trahair, N.S., Rasmussen, K.J.R., Finite-element analysis of the flexural buckling of columns with oblique restraints, *J Struct Eng,* 131(3), 481-487, 2005.
[23] Saha, G., Banu, S., Buckling load of a beam-column for different end conditions using multi-segment integration technique, *ARPN Journal of Engineering and Applied Sciences,* 2(1), 27-32, 2007.
[24] Galambos, T.V., *Structural Members and Frames*. Prentice-Hall International Inc,, New York, N.Y., 1968.
[25] López-Aenlle, M., Pelayo, F., Ismael, G., García Prieto, M.A., Fernández-Canteli, A., Buckling of laminated-glass beams using the effective-thickness concept, *Composite Structures,* 137, 44-55, 2016.
[26] He, J.H., Variational iteration method: a kind of nonlinear analytical technique, *Int J Nonlin Mech,* 34, 699-708, 1999.
[27] Coşkun, S.B., Atay, M.T., Determination of critical buckling load for elastic columns of constant and variable cross-sections using variational iteration method, *Computers and Mathematics with Applications,* 58, 2260–2266, 2009.
[28] Coşkun, S.B., Öztürk, B., *Advances in Computational Stability Analysis: (Chapter 6) Elastic stability analysis of Euler columns using analytical approximate techniques,* 115-132. Edited by Safa Bozkurt Coşkun, InTech ISBN No: 978-953-51-0673-9. DOI: 10.5772/45940, 2012.
[29] He, J.H., The homotopy perturbation method for solving boundary problems, *Phys Lett A,* 350, 87-88, 2006.
[30] He, J.H., An elementary introduction to the homotopy perturbation method, *Computers and Mathematics with Applications,* 57, 410-412, 2009.
[31] Coşkun, S.B., Determination of critical buckling load for Euler columns of variable flexural stiffness with a continuous elastic restraint using homotopy perturbation method, *International Journal of Nonlinear Sciences and Numerical Simulation,* 10, 187-193, 2009.

[32] Coşkun, S.B., Analysis of tilt-buckling of Euler columns with varying flexural stiffness using homotopy perturbation method, *Mathematical Modelling and Analysis,* 15(3), 275-286, 2010.
[33] Eryılmaz, A., Atay, M.T., Coşkun, S.B., Başbük, M., Buckling of Euler columns with a continuous elastic restraint via homotopy analysis method, *Journal of Applied Mathematics,* Article ID 341063 (8 pages), 2013.
[34] Adomian, G., *Solving Frontier Problems of Physics: The Decomposition Method,* Kluwer, Boston, MA, 1994.
[35] Yildirim, V., Numerical buckling analysis of cylindrical helical coil springs in a dynamic manner, *International Journal of Engineering & Applied Sciences,* 1, 20-32, 2009.
[36] Yildirim, V., On the linearized disturbance dynamic equations for buckling and free vibration of cylindrical helical coil springs under combined compression and torsion, *Meccanica,* 47, 1015-1033, 2012.
[37] Yildirim, V., Axial static load dependence free vibration analysis of helical springs based on the theory of spatially curved bars, *Latin American Journal of Solids and Structures,* 13, 2552-2575, 2016.
[38] Banerjee, J.R., Exact Bernoulli–Euler static stiffness matrix for a range of tapered beam-columns, *International Journal for Numerical Methods in Engineering,* 23(9), 1615–1628, 1986.
[39] Kacar, İ., Yildirim, V., Free vibration/buckling analyses of noncylindrical initially compressed helical composite springs, *Mechanics Based Design of Structures and Machines,* 44, 340-353, 2016.
[40] Tong, G., Zhang, L., A general theory for the flexural-torsional buckling of thin-walled members II: Fictitious load method, *Advances in Structural Engineering*, 6(4), 299-308, 2003.
[41] Rahai, A.R., Kazemi, S., Buckling analysis of non-prismatic columns based on modified vibration modes, *Communications in Nonlinear Science and Numerical Simulation,* 13(8), 1721-1735, 2008.
[42] Demir, C., Civalek, O., On the analysis of microbeams, *International Journal of Engineering Science*, 121, 14-33, 2017.
[43] Jalaei, M., Civalek, O., On dynamic instability of magnetically embedded viscoelastic porous FG nanobeam. *International Journal of Engineering Science*, 143, 14-32, 2019.
[44] Civalek, O., Dastjerdi, S., Akbaş, S.D., Akgöz, B., Vibration analysis of carbon nanotube-reinforced composite microbeams, *Mathematical Methods in the Applied Sciences*, https://doi.org/10.1002/mma.7069, 2020.
[45] Civalek, Ö., Avcar, M., Free vibration and buckling analyses of CNT reinforced laminated non-rectangular plates by discrete singular convolution method, *Engineering with Computers*, https://doi.org/10.1007/s00366-020-01168-8, 2020.
[46] Zhang, J., Ullah, S., Gao, Y., Avcar, M., Civalek, O., Analysis of orthotropic plates by the two-dimensional generalized FIT method, *Computers and Concrete*, 26(5), 421-427, 2020.
[47] Ding, Y., Hou, J., General buckling analysis of sandwich constructions, *Comput Struct,* 55(3), 485-493, 1995.
[48] Chakrabartia, A., Chalaka, H.D., Iqbala, M.A., Sheikhb, A.H., Buckling analysis of laminated sandwich beam with soft core, Latin American Journal of Solids and Structures, 9, 367–381, 2012.
[49] Magnucka-Blandzi, E., Magnucki, K., Effective design of sandwich beam with a metal foam core, *Thin-Walled Struct*, 45, 432-438, 2007.
[50] Jasion, P., Magnucki, K., Global buckling of sandwich column with metal foam core, *J Sandw Struct Mater,* 15(6), 718-732, 2013.

[51] Douville, M.A., Grognec, P.L., Exact analysis solutions for the local and global buckling of sandwich beam-columns under various loadings, *Int J Solids Struct,* 50, 2597-2609, 2013.
[52] Galuppi, L.G., Carfagni, R., Buckling of three-layered composite beams with viscoelastic interaction, *Composite Structures,* 107, 512-521, 2014.
[53] Grygorowicz, M., Magnucki, K., Malinowski, M., Elastic buckling of a sandwich beam with variable mechanical properties of the core, *Thin-Walled Structures,* 87, 127-132. 2015.
[54] Sayyad, A.S., Ghugal, Y.M., Bending, buckling and free vibration of laminated composite and sandwich beams, A critical review of literature, *Composite Structures,* 171, 486-504, 2017.

Appendix: Analytical Verification of the Results

Consider Eq. (16) at section $x = L$ for a beam without liners.

$$\boldsymbol{F}(L) = \begin{bmatrix} 1 & \frac{sin(\alpha L)}{\alpha} & \frac{cos(\alpha L)-1}{EI\alpha^2} & \frac{sin(\alpha L)-\alpha L}{EI\alpha^3} \\ 0 & cos(\alpha L) & -\frac{sin(\alpha L)}{EI\alpha} & \frac{cos(\alpha L)-1}{EI\alpha^2} \\ 0 & EI\alpha\, sin(\alpha L) & cos(\alpha L) & \frac{sin(\alpha L)}{\alpha} \\ 0 & 0 & 0 & 1 \end{bmatrix} \tag{A.1}$$

The elements of the transfer matrix given above is used for the expansion of the determinants given by Eq. (22) as follows

Beam with hinged ends

The expansion of the determinant leads to

$$|A|_{P-P} = \frac{sin^2(\alpha L)}{\alpha^2} - \frac{sin^2(\alpha L)}{\alpha^2} + \frac{\sin(\alpha L)\, L}{\alpha} \tag{A.2}$$

After simplification we are left with

$$|A|_{hinged-hinged} = \sin(\alpha L) = 0 \tag{A.3}$$

For $L \neq 0$ and $n = 0,1,2,3$ ... solution is found as

$$\alpha = \sqrt{\frac{N}{EI}} = \frac{\pi n}{L} \tag{A.4}$$

This gives

$$N = \frac{\pi^2 EI}{L^2}\, n^2 \tag{A.5}$$

Where $n = 0$ corresponds to the trivial solution. So, for a nontrivial solution, $n = 1$ should be taken to determine the critical buckling load of the beam with hinged ends.

$$(N_{cr})_{hinged-hinged} = \frac{\pi^2 EI}{L^2} \tag{A.6}$$

Beam with clamped-free ends

The following is used for the characteristic equation of the beam.

$$|A|_{clamped-free} = \begin{vmatrix} cos\,(\alpha L) & \frac{sin\,(\alpha L)}{\alpha} \\ 0 & 1 \end{vmatrix} = cos\,(\alpha L) = 0 \tag{A.7}$$

For $L \neq 0$ and $n = 0{,}1{,}2{,}3$ ... solution is

$$\alpha = \sqrt{\frac{N}{EI}} = (2n+1)\frac{\pi}{2L} \quad (n = 0{,}1{,}2, \dots) \tag{A.8}$$

From this we get

$$N = \frac{\pi^2 EI}{4L^2}\,(2n+1)^2 \tag{A.9}$$

The critical buckling load occurs when $n = 0$.

$$(N_{cr})_{clamped-free} = \frac{\pi^2 EI}{4L^2} \tag{A.10}$$

Beam with clamped-hinged ends

The expansion of the characteristic determinant gives

$$|A|_{clamped-hinged} = -\frac{sin(\alpha L) - \alpha L cos(\alpha L)}{EI\alpha^3} = 0 \tag{A.11}$$

Simplification leads to

$$tan(\alpha L) = \alpha L \tag{A.12}$$

There is no symbolic solution to this trascendental equation. It is satisfied to the four digits after period if the smallest root is taken as $\alpha L \cong 4.4934$.

$$tan(4.49341001) = 4.4934211571 \tag{A.13}$$

Therefore

$$\alpha L = \sqrt{\frac{N}{EI}} L \cong 4.4934 \tag{A.14}$$

or

$$(N_{cr})_{clamped-hinged} = \frac{20.19064356\, EI}{L^2} = 2.046\, \frac{\pi^2 EI}{L^2} \tag{A.15}$$

is obtained.

Beam with clamped ends

For C-C ends we have

$$|A|_{C-C} = 2 - L sin(L\alpha) - 2cos\,(L\alpha) = 0 \tag{A.16}$$

or

$$|A|_{C-C} = 4sin^2\left(\frac{L\alpha}{2}\right) - \alpha L\, sin(L\alpha) = 0 \tag{A.17}$$

By using the following trigonometric identity

$$sin(L\alpha) = 2\, sin\left(\frac{L\alpha}{2}\right) cos\left(\frac{L\alpha}{2}\right) \tag{A.18}$$

The expansion of the determinant reduces to

$$|A|_{C-C} = sin\left(\frac{L\alpha}{2}\right)\left\{4sin\left(\frac{L\alpha}{2}\right) - 2\alpha L cos\left(\frac{L\alpha}{2}\right)\right\} = 0 \tag{A.19}$$

From this we get the solution as follows

$$sin\left(\frac{L\alpha}{2}\right) = 0 \tag{A.20}$$

or

$$\frac{L\alpha}{2} = \frac{L}{2}\sqrt{\frac{N}{EI}} = n\pi \quad (n = 1,2,\dots) \tag{A.21}$$

If the axial load is isolated from the above

$$N = \frac{4\pi^2 EI}{L^2}\, n^2 \quad (n = 1,2,\dots) \tag{A.22}$$

The corresponding critical load is obtained for $n = 1$ as in the following.

$$(N_{cr})_{C-C} = \frac{4\pi^2 EI}{L^2} \tag{A.23}$$

It is revealed that this critical load is exactly quadruple of the pinned-pinned Euler column. Thus fixing two ends has increased the critical load to a large extent.

International Journal of Engineering & Applied Sciences (IJEAS)
Vol. 13, Issue 1 (2021) 36-42
http://dx.doi.org/10.24107/ijeas.879095
Int J Eng Appl Sci 13(1) (2021) 36-42

Effect of Frequency on Eddy Losses of Transformers

Yıldırım Özüpak

Dicle University Silvan Vocational School, Electrical and Energy Department, Diyarbakır, Turkey
E-mail address: yildirim.ozupak@dicle.edu.tr

ORCID numbers of author:
0000-0001-8461-8702

Received date: 12.02.2021
Accepted date: 08.03.2021

Abstract

Transformer is a vital component of electrical power systems for transmission and distribution. Robust design to increase the efficiency of a transformer is one of the main factors in transformer manufacturing. The efficiency of a practical transformer is limited by the losses caused by design and manufacturing defects. Losses in transformers can be divided into idle losses and losses under load. Eddy current loss is obtained from the idle losses of the transformer. In this paper, the effect of eddy effect causing HV energy loss at high magnetization frequencies was investigated. ANSYS@Maxwell software based on the Finite Element Method was used to analyze the eddy current loss in a T-connected, 3-leg and 3-phase distribution transformer of 15 MVA. The losses are obtained from no-load tests by changing the operating frequency of the transformer. Depending on the frequency value in the range of 50-60 Hz, the change in eddy current loss has been observed while the transformer winding is excitation at 1.74 T magnetic flux density. It has been observed that increasing the frequency causes an increase in the no load loss in the 3-phase transformer.

Keywords: Transformer, FEM, Frequency, Magnetic field, Eddy current loss.

1. Introduction

Calculating the parameters of power transformers, designing, modeling and realizing lifelike simulations of these transformers has always been a challenge for designers. These transformers are the most expensive item of energy transmission and distribution facilities. For this reason, it has always been important for designers to predict the correct operation of the transformer and to know the possible failures that may occur. They performed the study and analysis of high frequency models of power transformers for the analysis of the transient interaction between power systems and transformers [1]. It realizes the identification of different internal faults that cause power cuts in transformers with an algorithm and transformer model [2]. In recent years, with the development of computer software programs, different nonlinear core materials used in transformers core and simulation programs based on Finite Element Method (FEM) have been used intensively to model the permanent magnetization of these materials [3]. ANSYS @ Maxwell based on FEM was used to calculate the parameters of the model transformer in discharges occurring in the windings of transformers [4]. Mains frequency controlled or uncontrolled rectifiers used in power electronics draw currents containing harmonic components from the electric grid. The loss of transformers in the no-load state consists of eddy and hysteresis losses. [5]. The effect of eddy loss on transformer loss can be calculated as:

$$P_e = kB_{max}^2 f^2 \tag{1}$$

K: constant

B: maximum flux density

F: frequency

The losses occurring in the transformer's magnetic core reach high values at high frequencies [6]. It shows that by using ferromagnetic material in a transformer core model, the core loss increases with increasing frequency [7].

Eddy currents become negligible at very low magnetization frequency. This allows a method is as shown in Fig. 1. A summary of the core loss mechanism is given in Fig. 2.

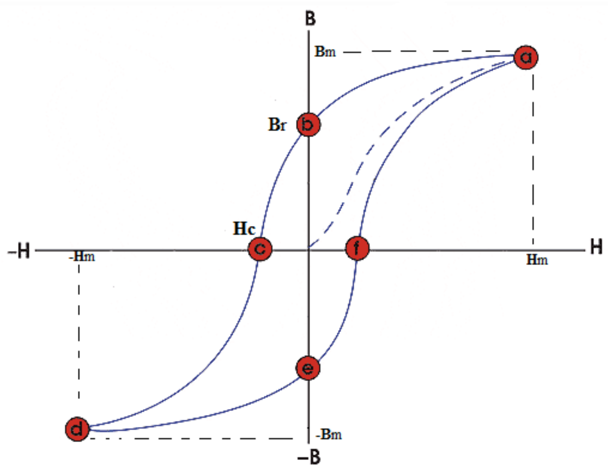

Fig. 1. Hysteresis curve of magnetic materials

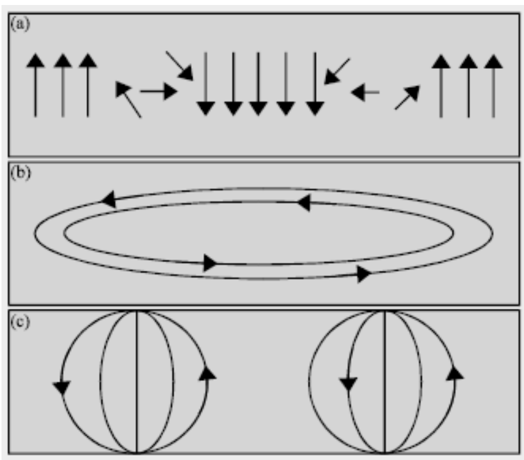

Fig. 2. Core loss summary.

The power loss of no load transformer may be written as [6]:

$$P_T = P_h + P_e + P_a \tag{2}$$

Eddy currents in transformer cores can be minimized. This reduces the conventional eddy current losses that are highly based on core material thickness [8,9].

2. Material and Method

The main component core consists of a three-legged three-phase 15 MVA transformer core with a T-joint shear angle. The characteristics of the transformer are given in Table 1.

Table 1. Properties of Transformer

Parameter	Value
Rated Power	15.MVA
HV	33.000 V
LV	11.000 V
Frequency	50 Hz
HV turn number	665
LV turn number	128
Material	M125-027S
Material thickness	0.3 mm
Conductivity	5000000 S/m
Stacking factor	0.95

In core type transformer, both primary and secondary windings are placed on side limbs. This type of transformer has two magnetic circuits. Fig. 3 shows the prototype of the core type transformer designed.

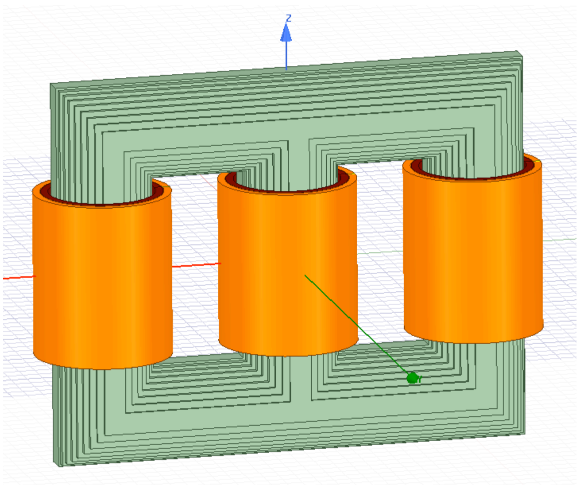

Fig. 3. Core type three-phase transformer.

In the transformer model, the boundary conditions are defined on the external geometry and properties of all materials. The magnetic core is characterized by thin laminations such as the B-H curve of magnetization given in Fig. 4 [1-2].

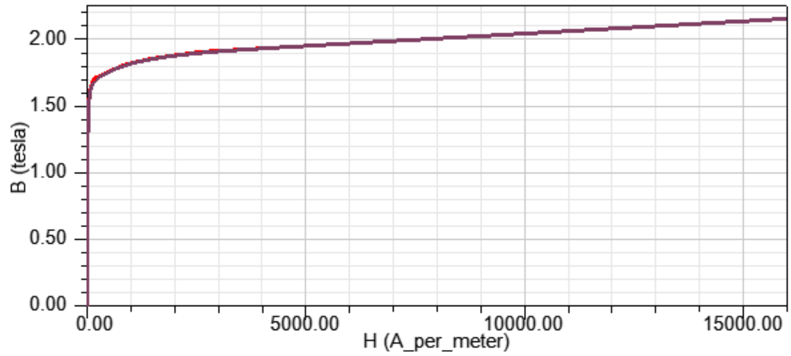

Fig. 4. B-H curve of core material

In order to eliminate sudden currents and shorten the simulation time, exponential excitation is given as given in Fig. 5.

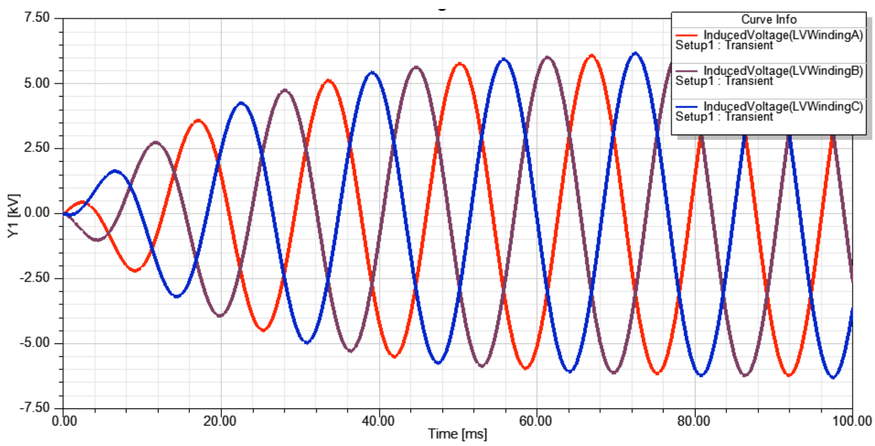

Fig. 5. Transformer excitation voltage curve

In order to analyze the designed model, the entire model is divided into many elements, usually triangles. The mesh (mesh) of the model created with finite elements is presented in Fig. 6.

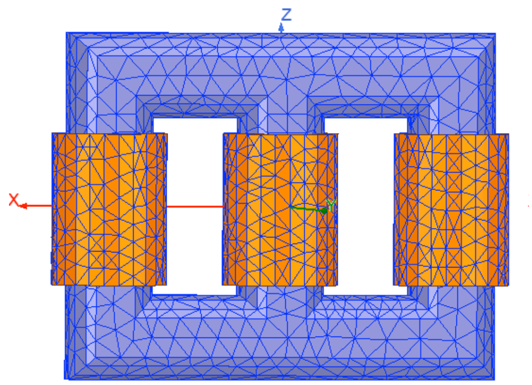

Fig. 6. Mesh of transformer.

Testing has been done using the no-load test test. Each winding is also designed so that the stepped length of the three phase core can be varied.

3. Analysis and Results

The magnetic flux distribution of the designed transformer model at 50 Hz frequency and depending on the variable magnetic field is given in Figure 7.

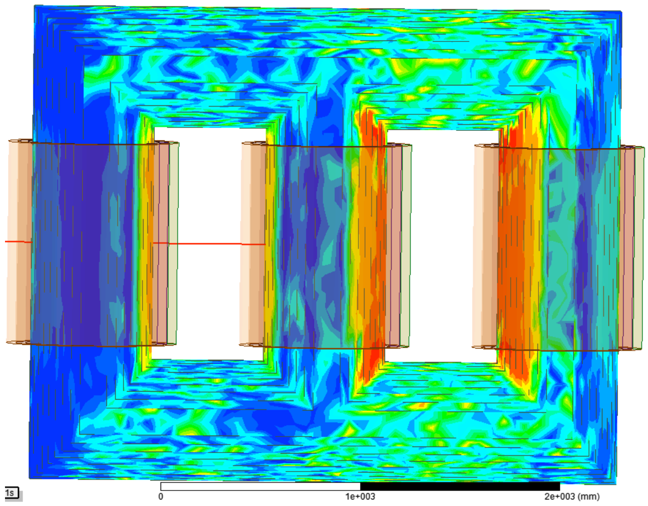

Fig. 7. Magnetic flux distribution.

The variation of the eddy current loss in three phase cores is presented in Figure 8. As a result of this research, it was seen that the core loss was 12.41 kW. The loss in this study is the classical eddy current. Table 2 shows the eddy current loss variation obtained from the simulation.

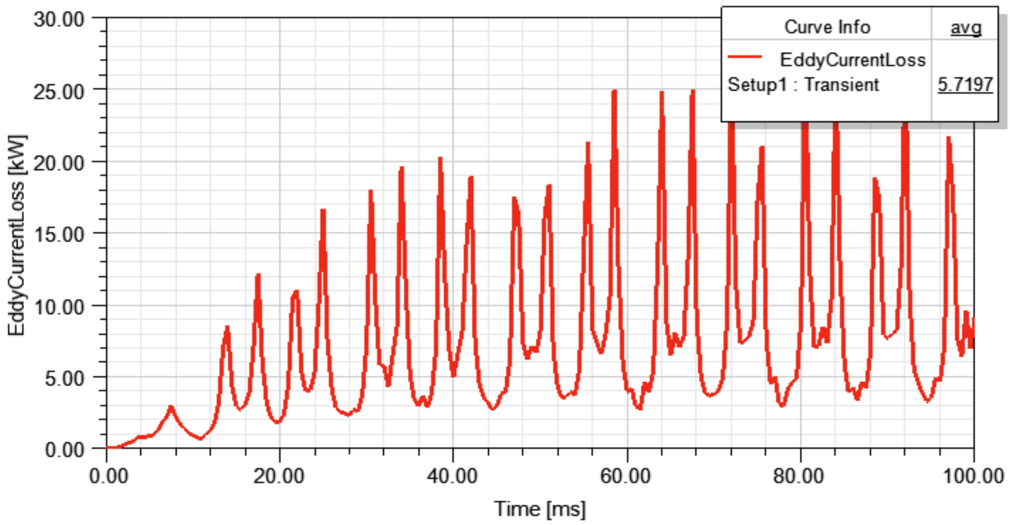

Fig. 8. Eddy current loss at 50 Hz frequency

Table 2. Variation of eddy current loss with frequency

Frequency (Hz)	Eddy Current Loss (kW)
50	5.748
52	5.931
54	6.121
56	6.218
58	6.355
60	6.421

In cases where the frequency increased, the eddy current loss increased. It can be clearly stated that there is much about eddy current losses in the literature. When the flow, flux density and frequency value of the flux in the junctions increase, due to the movement of the flux, there is an air gap between the joints, so the flux adhering to the joint and this will allow the magnetic flux to flow to the other electrical steel lamine. Flux will be circulated in the field as shown. As a result, it has been seen how eddy current losses increase depending on the increase in frequency.

7. Conclusions

In this paper, from the results of the model analyzed at 50 Hz frequency, it was seen that the lowest power loss of the transformer core, ie eddy current losses, has a significant effect on the total core losses of the idle 3-phase transformer. The increase in frequency has caused an increase in transformer core losses. The eddy current losses on the core also varied depending on the change of magnetic flux. As a result, it has been seen how eddy current losses increase depending on the increase in frequency.

Acknowledgments

This study was supported by Inonu University Scientific Research Projects Coordination Unit. Project Number: FBA-2017-639.

References

[1] Özüpak, Y., Mamiş, M.S., Realization of electromagnetic flux and thermal analyses of transformers by finite element method, *IEEJ Transactions on Electrical and Electronic Engineering*, 14(10), 1478-1484, 2019.

[2] Morched, A., Marti, L., Ottevangers J., A high frequency transformer model for the EMTP, *IEEE Transactions on Power Delivery*, 8(3), 1615-1626, 1993.

[3] Özüpak, Y., Mamiş, M.S., Teke, İ.H., Electromagnetic field and total loss analysis of transformers by finite element method, *International Journal of Engineering And Computer Science*, 8(1), 24451-24460, 2019.

[4] Özüpak, Y., Mamiş, M.S., Realization of electromagnetic flux and thermal analyses of transformers by finite element method, *IEEJ Transactions on Electrical and Electronic Engineering*, 14(10), 1478-1484, 2019.

[5] Subedi, D., Lightning induced over-voltages in power transformer and voltage spikes in connected load, Master Thesis, Aalto University, Helsinki, Finland, 2017.

[6] Shirvani, A., Malekian, K., Schmidt, U., Schufft, W., A New Power transformer Model Over Wide Frequency range for EMTP, *45th International Universities Power Engineering Conference UPEC2010*, 1-6, 2010.

[7] Sabiha, N.A., Lightning-induced overvoltages in mediumvoltage distribution systems and customer experienced voltage spikes, PhD Thesis, Aalto University, Helsinki, Finland, 2010.
[8] Shareghi, M., Phung, B.T., Naderi, M.S., Blackburn, T.R., Ambikairajah, E., Effects of current and voltage harmonics on distribution transformer losses, *International Conference on Condition Monitoring and Diagnosis (CMD)*, 633-636, 2012.
[9] Soh, T.L.G, Said, D.M., Ahmad, N., Nor, K.M., Salim, F., Experimental study on the impact of harmonics on transformer, *IEEE 7th International Power Engineering and Optimization Conference (PEOCO),* 686-690, 2013.